國立交通大學

電控工程研究所

碩 士 論 文

應用於有機垂直奈米接面氣體感測器之全自動讀取電路設計

An Automatic Readout Circuit for an Organic Vertical Nano-junctions Gas Sensor

研 究 生：陳弘哲

指導教授：趙昌博 教授

中 華 民 國 一 百 零 二 年 七 月

應用於有機垂直奈米接面氣體感測器之全自動讀取電路設計

An Automatic Readout Circuit for an Organic Vertical Nano-junctions Gas Sensor

研 究 生　：陳弘哲　　Student：Hung-Che Chen

指導教授　：趙昌博　　Advisor：Paul C.-P. Chao

國 立 交 通 大 學

電 控 工 程 研 究 所

碩 士 論 文

A Thesis

Submitted to Department of Electrical and Control Engineering

College of Electrical and Computer Engineering

National Chiao Tung University

in partial Fulfillment of the Requirements

for the Degree of Master

in

Electrical and Control Engineering

July 2013

Hsinchu, Taiwan, Republic of China

中 華 民 國 一 百 零 二 年 七 月

應用於有機垂直奈米接面氣體感測器之全自動讀取電路設計

學生：陳弘哲　　指導教授：趙昌博

國立交通大學 **電機與控制工程研究所** 碩士班

摘要

本論文提出的新穎氣體讀取電路是特別針對有機垂直奈米接面二極體氣體感測器作設計，利用此設計電路整合前端氣體感測器成為氣體感測系統。讀取系統包含七個部份，第一部份為前置放大器，此前置放大器由轉阻放大器構成，目的為將氣體感測器的輸出電流轉成電壓變化。第二部份為峰值偵測保持電路，此電路將偵測最大電壓並維持住這個值，也就是初始值。第三部份為除法器，其目的為計算出氣體感測元件之飽和電流和初始電流的比例。第四部份為飽和偵測電路，用以偵測感測器輸出電流何時不再變化(也就是反應達飽和)。第五部份為自動重置電路，用來偵測感測器何時開始與氣體反應並重置峰值偵測保持電路的電壓值。第六部份為邏輯閘和緩衝器，當感測器正與氣體反應且反應達飽和時，透過邏輯閘和緩衝器輸出結果，否則顯示為零。第七部份為微處理器，使用的是 ALIENTEK 公司的 STM32，中央處理器為 ARM Cortex ™-M，我們使用到其中的類比數位轉換器作類比感測電路輸出結果的轉換，然後 LCD 顯示結果。本電路利用台積電 0.35μm 2P4M 3.3V 混合訊號互補式金氧半導體製程將特別設計的電路由 IC 實現。研究晶片經由財團法人國家實驗研究院晶片系統設計中心贊助，三次設計的晶片面積分別為 1.083×1.04 mm^2 、1.082×1.082 mm^2 以及 0.74×0.75 mm^2。本系統結合前端感測器作模擬氣體感測器之輸出電流量測，已實際測試其可行性。不同於傳統儀器的量測環境，此氣體感測系統的設計，具有即時偵測、攜帶方便、成本低廉與降低人為誤差的優勢，能確實賦予生醫感測器在居家醫療方面所帶來的價值。

關鍵字：有機垂直奈米接面二極體、前置放大器、峰值偵測保持、類比除法器、氣體感測系統。

An Automatic Readout Circuit for an Organic Vertical Nano-junctions Gas Sensor

Student: Hung-Che Chen Advisor: Paul C.-P. Chao

Institute of Electrical and Control Engineering
National Chiao Tung University

ABSTRACT

A novel readout circuit for a gas sensor based on an organic diode with vertical nano-junctions (VNJ) is proposed in this study. There are seven parts included in the readout system. First part is a preamplifier, which is composed of trans-impedance to convert the output current of a gas sensor into voltage. Second part is a peak-detect-and-hold circuit. It can detect the maximum voltage and holds its value, the initial value. Third part is a divider, which is used to calculate the ratio of saturation current to initial current. Fourth part is the saturation detector, which is used to detect when the output current of the VNJ-P3HT diode doesn't change anymore (that is, the responses are saturated). Fifth part is the auto-reset circuit, which is used to detect when the sensor device starts to react with gas and reset the voltage value of the peak detect-and-hold circuit. Sixth part is a logic gate and a buffer. When the sensor device is reacting with gas and the responses are saturated, the response result is outputted through the logic gate and buffer. Otherwise, the zero is outputted. Seventh part is a micro-processor control unit (MCU). STM32 is the CPU of proposed MCU by ALIENTEK. The ADC of MCU is used to transform the output data of readout circuit. Then the LCD displays the results. The designed circuit is accomplished by Taiwan Semiconductor Manufacturing Company (TSMC) 0.35μm 2P4M 3.3V mixed-signal

CMOS process. The proposed chips with the die area of 1.083×1.04 mm^2, 1.082×1.082 mm^2 and 0.74×0.75 mm^2 are fabricated by National Applied Study Laboratories National Chip Implementation Center (NARL NCIC). The output current of front-end gas sensor is simulated and the experimental results show the sensing system is workable. The design of the proposed readout circuit provides benefits of detection speed, portability, low-cost and less human operational errors compared with the measurement by traditional instruments. Thus the added value is brought for bio-sensors and applied in home care.

Keywords: Organic diode with vertical nano-junctions (VNJ), Preamplifier, Peak-detect-and-hold, Analog Divider, and Gas Sensing System.

ACKNOWEDGEMENTS

本論文得以順利完成，首先要對我的指導老師趙昌博教授表達感激之意。老師在我碩士就讀期間除了在研究上給予我指導外，並教導我們面對問題的正確態度，碩士生涯在此氛圍中，使我成長與茁壯。對於實驗室的博班學長姊們，杜哲怡、莊煒宜、高永原、李奎佑、蔡哲弘、陳緯達、程俊凱，以及上屆的學長們，林上智、陳建瑞、黃子嘉、林偉竹、徐彥平、吳若華所提供鼓勵與建議表達感謝。感謝我的同學江昭德、管清華、蔡鴻銘、曾德修彼此之間互相扶持，此將成為碩士生涯中重要的篇章。感謝實驗室的學弟孫祥方、彭玄文、張鈞凱、李誌偉、吳承泰、Hieu、蘇家偉帶來實驗室輕鬆愉快的氣氛，為碩士生活增添一筆活潑的色彩。感謝光電所冉曉雯老師和戴銘志學長在執行計畫時所給予的協助，使我在執行計畫時更為順利。

感謝我的家人，爸爸、媽媽和弟弟，在我就讀期間給我的體諒與寬容、支持與鼓勵，使我無後顧之憂地完成學位，對於你們的感恩之情難以言表。

感謝我的指導老師趙昌博，以及我的口試委員黃聖傑和甘堯江老師在口試時給予的建議。最後感謝我在碩士期間遇到的所有朋友，由衷感謝你們讓我的碩士生涯能夠多采多姿。

CONTENT

TABLE CAPTIONS

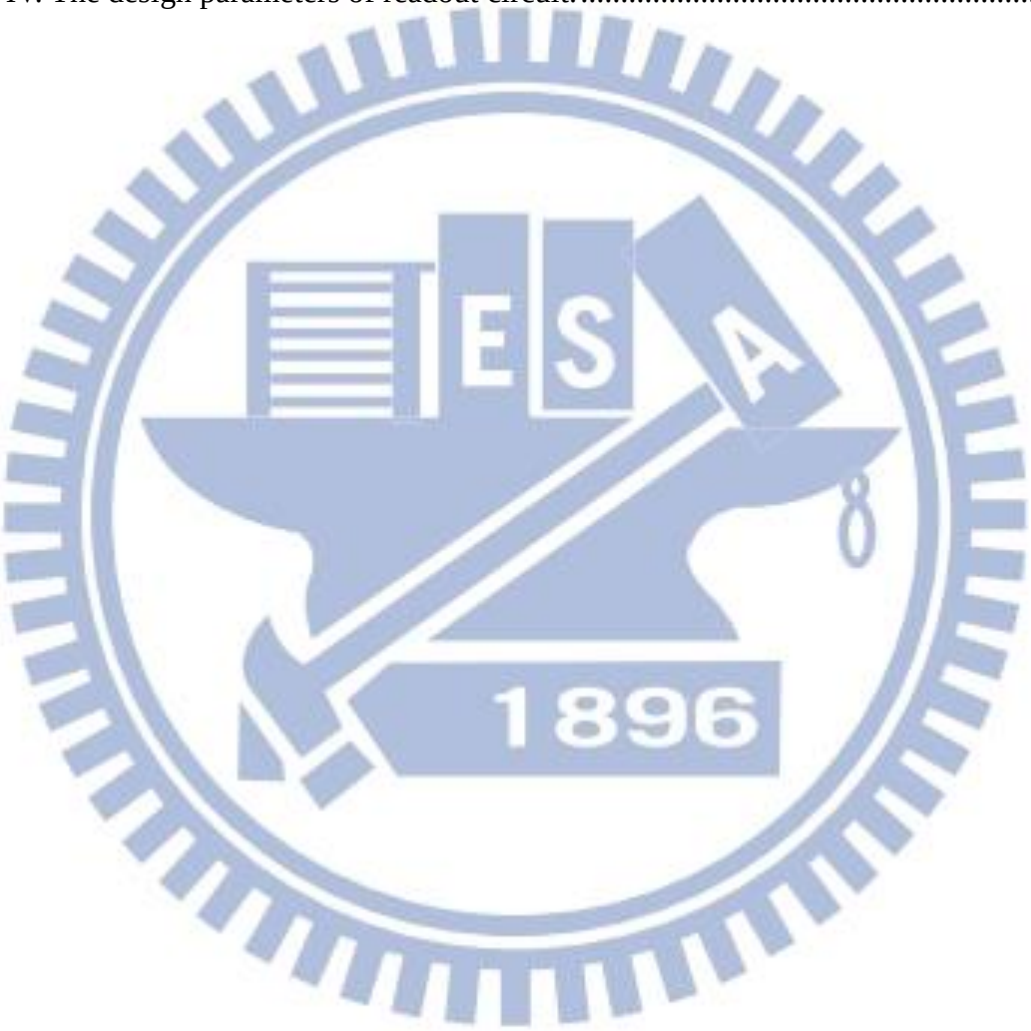

FIGURE CAPTIONS

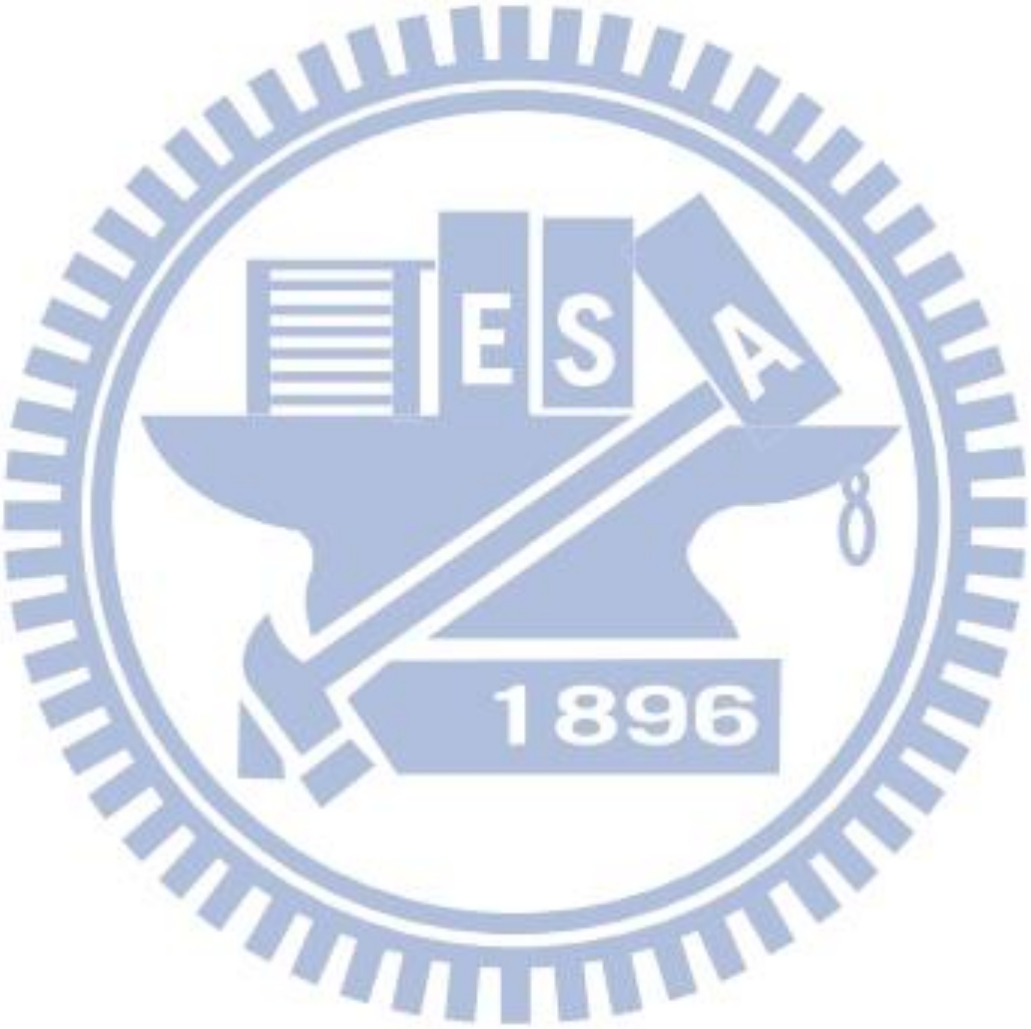

CHAPTER 1

Introduction

1.1 Motivation

Bio-chips are a valuable medical application. A bio-chip is a collection of miniaturized test sites (micro-arrays) arranged on a solid substrate that permits many tests to be performed at the same time in order to achieve higher throughput and speed. Researchers use bio-chip to quickly screen large numbers of biological analyses for a variety of purposes, from disease diagnosis to detection of bioterrorism agents. The bio-chip owns the advantages of light weight, detection speed, low-cost, portability, disposability and less human operation errors, for examples of new drug development, clinical disease testing, strain screening and so on.

Integrating the device and associate circuit in a single chip is the development goal of the bio-chip. The advantages of equipping the integrated circuits with the CMOS-MEMS process are commonly applied in commercial and academic usages. The integrated system is called Bio-MEMS. The sensor can be either measured directly or implemented by commercial IC to be integrated into the systematic applications, even though it fabricated by a non-CMOS process. But it is not able to reach aims of portability and speedy response. Thus the disadvantage of direct measurement is inconvenience.

The proposed method of integrating the circuit into a single chip is able to be adapted to every sensor component while bringing less noise than the method of using commercial IC to measure. Non-invasive, disposable and light-weight sensors for detecting ammonia concentration in patient mouth are in high demand nowadays, suggested by clinical doctors. More than two hundred kinds of gas substances exhaled from a human mouth are detected and reported in past studies, some of which is associated with disease. There is a great potential for further development in utilizing human’s outhaul air for diagnosis. The readout circuits are

designed on the basis of characteristic of gas sensors. Meanwhile, it constructs a novel bio-sensor system.

1.2 Types of Ammonia Gas Sensors

Ammonia is a colorless gas with a characteristic pungent smell. Nitrogen plus hydrogen yield ammonia with the formula NH_3. It is used as fertilizer above eighty percent and one of the well-known inorganic compounds in the world. Ammonia plays an important role for food industry and agricultural industry. It is wide-range in applications. Ammonia is also a building-block for the synthesis of many pharmaceuticals and is used in many commercial cleaning products. However, ammonia harms the respiratory of animal and human and is causticity and irritating to skin. Thus exposing to excess ammonia for a long time is a health risk to people.

Ammonia is one of more than two hundred kinds of gas substances in the breath of human. The ammonia odor could be linked to liver and kidney malfunction in exhaled breath. Ammonia therefore has effect on prevention of disease in biomedical opinion. It is usually asymptomatic in the early stages in chronic liver disease. Consequently, it is recommended that patients with a history of hepatitis or hepatitis virus carrier regular monitor liver function. The prognosis of hepatic fibrosis can be improved if early diagnosis and may reduce risk of development of sever conditions such as cirrhosis or cancer since the early fibrotic changes are reversible. The levels of blood ammonia are increased (hyperammonemia) and the breath of these patients may have an ammonia-like odor because of liver cell damage. Thus detecting breath ammonia to monitor liver disease is one critical issue when developing point-of-care technology. The development of point-of-care applications is limited because a simple, reliable, portable, and low-cost breath ammonia sensor is not commercialized. In order to detect ammonia concentration accurately, more and more people investigate ammonia gas sensor in recent years. Many types of ammonia gas sensor are designed on the basis of

different sensor principles.

1.2.1 Resonance Sensors

In order to detect target gases, quartz crystal microbalance (QCM) sensor [1] and surface acoustic wave (SAW) [2, 3] are coated with membranes on chemical interfaces. The chemically selective coating on the sensor surface absorbs the mass of object. The resonant frequency of the sensor is changed by mass loading caused absorption of specific gas.

QCMs are one of acoustic wave techniques. It response to small mass changes on the surface when the sensing films interact with target gas. QCMs are widely used in sensor devices for its linearity, durability and high sensitivity. The shift of resonant frequency is caused by the adsorption of the gas molecules onto the thin membranes.

The SAW sensors apply piezoelectric materials as substrate. Two sets of inter digital transducer (IDT) were manufactured on the substrate. One of them is received electrical signals that convert to SAW through converse piezoelectric effect and regarded as input. SAW devices can satisfy, accuracy, good reliability, high sensitivity, competitive pricing and real-time measurement. The other is treated output that transforms SAW through piezoelectric effect into electrical signal. In order to analyze target gas between the two IDTs, the sensor region is coated with membranes. The changes in SAW velocity can be evaluated by measuring the frequency shift of SAW and caused by the mass loading effect.

1.2.2 Optic Absorption and Ultrasonic Detection Sensors

Absorbing light at different region of wavelength by different gases is the main principle of a fiber-optic sensor [4, 5]. Monitoring magnitude of absorption signal and making certain peak absorption wavelength are based on ammonia concentration. In order to increase the sensitivity and selectivity of the sensor, some optical fiber as transducer coated on the surface purposes.

The time-of-flight (TOF) method calculate propagation velocity of ultrasonic at the same

distance in different concentrations of gas and is called ultrasonic detection [6]. According to odds on reference gas and target gas, the gas concentration can be determined. When molecular weight of specific gas is different largely from air, the measurement has the better performance. It contrasts with the chemic sensor in regard to problems of the short sensor life and the secondary pollution.

1.2.3 Transistors Sensors

In order to construct the gate of transistor, the different chemical interfaces are deposited on top of the insulator. Several ammonia gas sensors depend on different chemical interfaces such as metal [7], metal-oxide [8] and polymer film [9]. The drawback of metal-oxide film's operational temperature is high and metal film's dynamic range is narrow. But polymer film can detect selectivity at room temperature. After the interface of those films interacts with the NH_3 molecules, the chemical reactions can affect charge carrier density of transistors. The conductivity of material and the resistance of film are changed by the result.

Organic thin film transistors (OTFT) [10] own the advantages of flexible, disposability, large-area, popular prices and operating at room temperature compared with inorganic field effect transistors (FET). But the challenges of the OTFT sensor are the reliability and repeatability. Thus a new gas sensor made of a novel organic diode with vertical nano-junctions (VNJ) is presented, which is more convenient for diagnosis of biomedical than the OTFT sensor.

1.3 Reference Review of Gas Sensor Readout Circuits

Because output signal of sensor component is current, the readout circuit is in the trans-impedance type on the first state. An example of trans-impedance is the capacitive trans-impedance amplifier (CTIA), which is composed of a feedback capacitance and operational trans-conductance amplifiers (OTA) [11-15]. A dominant advantage of great performance on high frequency is in this framework. Because of response time of the gas sensor, the readout

circuit does not operate on high frequency. In order to stabilize dc bias, some of them also use common mode feedback (CMFB) technology [14, 15]. However, the CMFB technology is usually applied to fully differential amplifier. In view of above mentioned reasons, the referred structure is not suitable to use in the readout circuit.

For another example, the trans-impedance amplifier uses a feedback resistance direct [16]. In order to convert currents into voltages, the previous design is designed with the similar way. The obvious problems on impedance matching and noise are direct generated by the way of feedback resistance.

Unlike other references, the circuit frame does not need the operational amplifier to convert currents into voltages [17]. Because the gain of the TIA approximates feedback resistance, the gain of the TIA can be adjusted for different experiment environments. It is different from the gas sensor in this study because the framework does not bias sensor components. In this readout circuit, biasing the gas sensor is included in the function of the TIA.

1.4 Overview of This Thesis

Introducing the principle of sensing method for ammonia sensors is in the first chapter. The ammonia sensors based on an organic diode with vertical nano-junctions (VNJ) are presented in the second chapter. There are the experimental data for the relation between concentration of ammonia and response of ammonia sensors. Then introducing the principle of readout system, which is proposed to acquire and process the signals, which are attributable to ammonia concentration in the third chapter. And the theory and framework of the readout circuit are described. In the fourth chapter, the simulation results and measurement data of the sensing circuit are shown and discussed. Finally, the results of the research are summarized, and moreover, the potential applications and future works are proposed in the fifth chapter.

CHAPTER 2

Performances and Characteristics of Gas Sensors for Ammonia

2.1 Characteristics of Pentacene-based OTFT

Mobility of inorganic material is greater above three orders compared with mobility of organic material. In organic thin film material, pentacene thin film has the best mobility at present. The structure and electric characterization of the particular OTFT are introduced in this section.

2.1.1 Structure of Pentacene-based OTFT

The substrates of OTFT are made of the silicon material. The insulator on the second level and gate electrode is SiO_2. PMMA [poly(methyl methacrylate)] was used as the buffer layer to improve electric characteristics of SiO_2 dielectric surface [18]. The dipole moment of PMMA

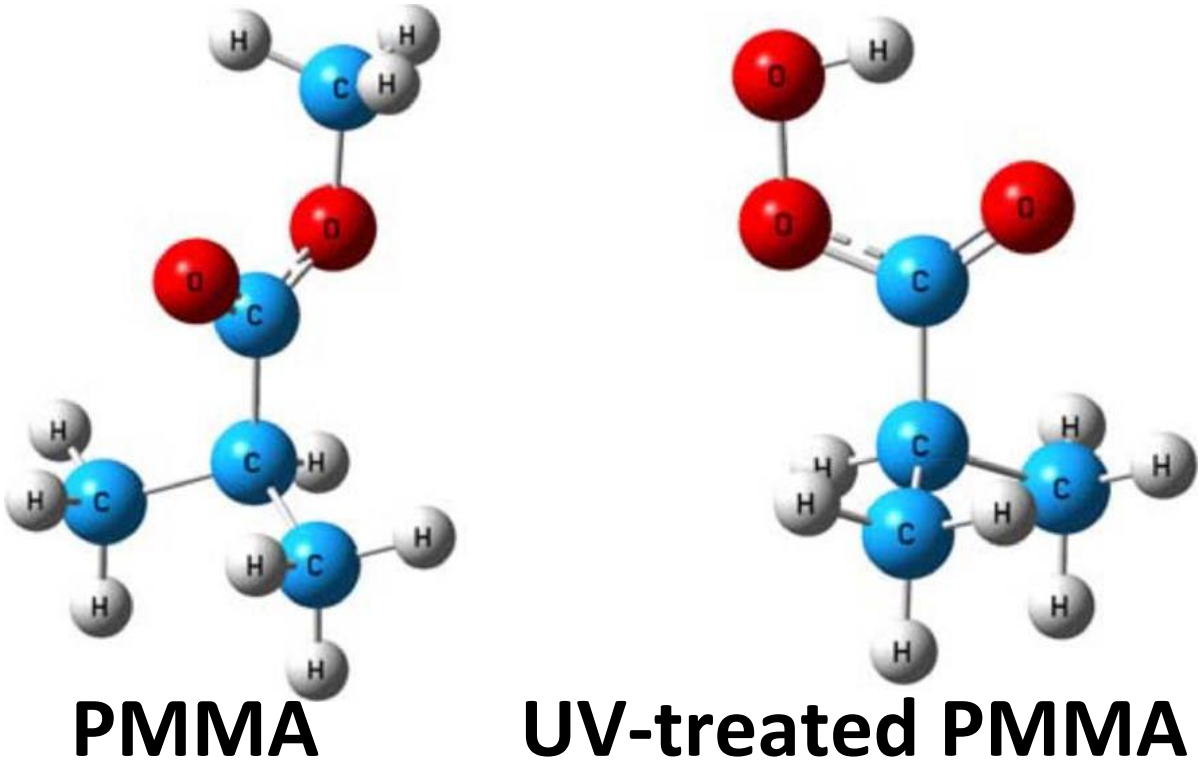

Fig. 1. Functional end-groups of PMMA and UV-treated PMMA [18].

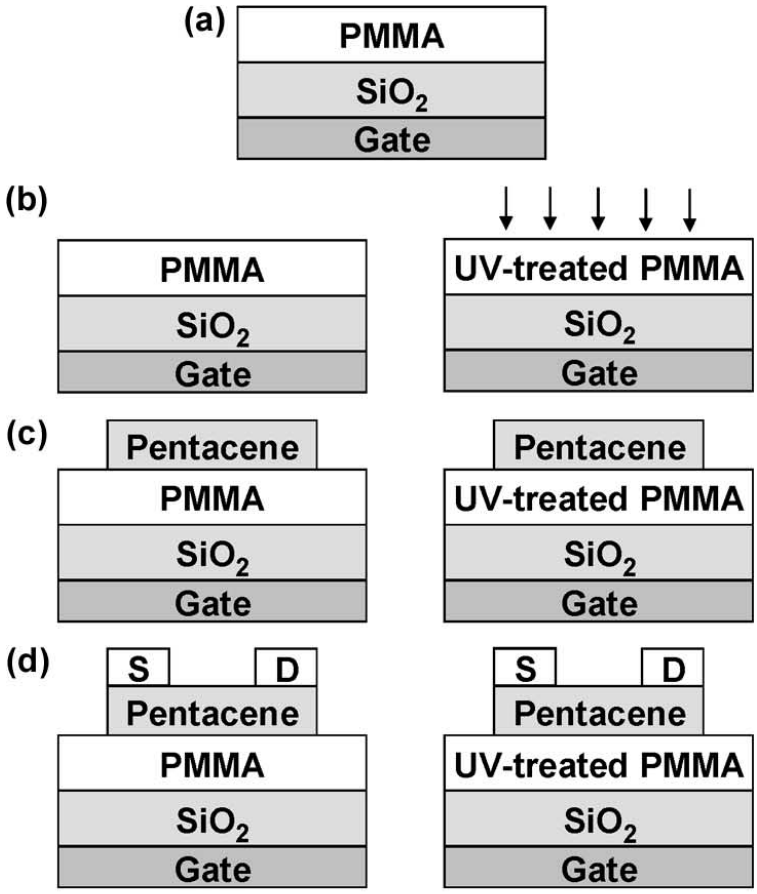

Fig. 2. Fabrication and structure of pentacene-based OTFT [18].

end-groups are increased because part of the SiO_2 with PMMA was irradiated by UV-light (shown in Fig. 1). After being deposited on the PMMA dielectrics, the pentacene film was evaporated to form the active layer. The source and drain contacts are made by depositing the gold film through a shadow mask. Fig. 2 shows the flowchart for the fabrication processes of the proposed pentacene-based OTFT.

2.1.2 Electric Characterization of Pentacene-based OTFT

Because the development of OTFT has not yet completed, modeling OTFT has not yet been realized. In order to analyze OTFT's electric characterization in a wide range, the formula of electric characterization for metal-oxide-semiconductor field-effect transistors (MOSFETs) are used. When the OTFT are operated in triode region, the drain current (I_d) of OTFT can be expressed as

$$I_d = \mu C_{ox} \frac{W}{L}\left[\left(V_g - V_{th}\right)\cdot V_d - \frac{1}{2}V_d^2\right], \quad (1)$$

where μ is the charge-carrier effective mobility, C_{ox} is the gate oxide capacitance per unit area, W is the gate width and L is the gate length. Simplification of Eq. (1) shows Eq. (2) when $V_d << (V_g\text{-}V_{th})$,

$$I_d = \mu C_{ox} \frac{W}{L}\left(V_g - V_{th}\right)\cdot V_d . \quad (2)$$

In saturation region, the drain current response of OTFT is defined as

$$I_{d,sat} = \frac{1}{2}\mu C_{ox} \frac{W}{L}\cdot\left(V_g - V_{th}\right)^2, \quad (3)$$

$$\left(I_{d,sat}\right)^{\frac{1}{2}} = \left(\frac{1}{2}\frac{W\mu}{L}C_i\right)^{\frac{1}{2}}\cdot\left(V_g - V_{th}\right). \quad (4)$$

Because the mobility of MOSFET is much larger than the mobility of OTFT, the current of drain-source on OTFT is much less than that on MOSFET. In order to increase the output current of OTFT, enlarging the gate width and/or decreasing the gate length are one of the methodologies. The results can be used in increasing response at the same ammonia concentration.

2.2 Ammonia Sensing Responses of Pentacene-based OTFT

2.2.1 Primary Parameters of Pentacene-based OTFT

Turn-on current, threshold voltage (V_{TH}), intrinsic mobility (μ) and sub-threshold slope (*S.S.*) are the significant variations of OTFT. When transistors are turned on, the maximum drain current is called turn-on current. When channel forms at the interface between the insulating layer and the substrate of the transistor, the gate voltage is defined as threshold voltage. The ability of driving charged particles under an applied electric field is intrinsic mobility. In order to make a low resistance conducting path between the drain and source, there are sufficient carriers in the channel. The device performance is better because of higher mobility. Sub-threshold slope is defined as

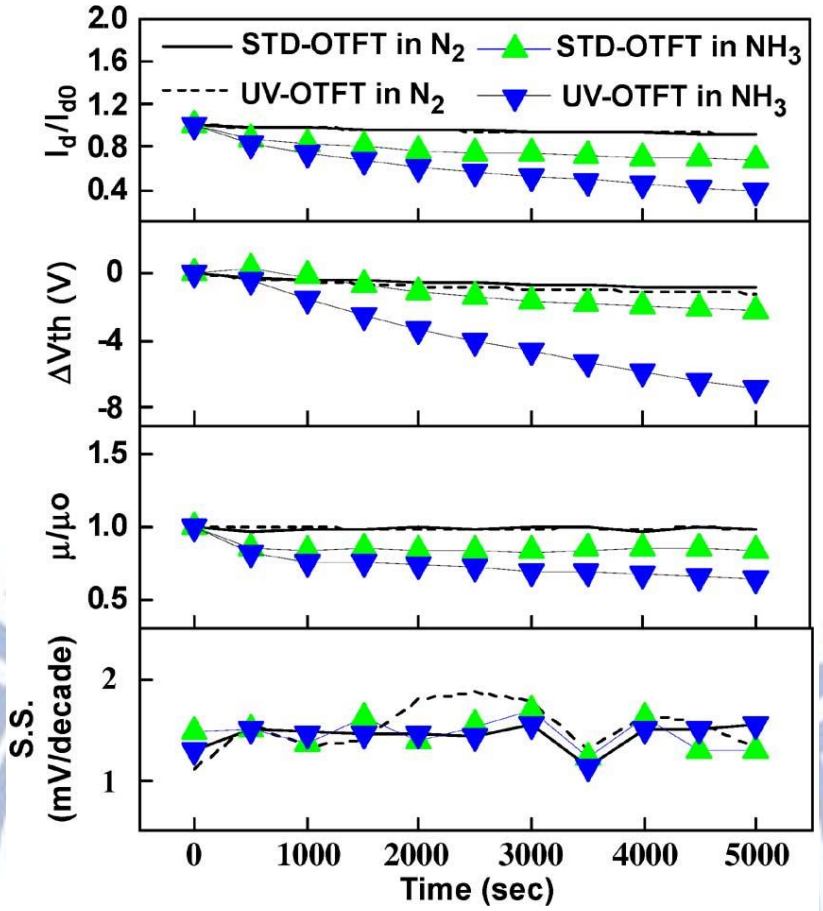

Fig. 3. Parameters versus time plot of STD and UV-OTFT in nitrogen and ammonia conditions [18].

$$SS = \left[\frac{\partial (\log I_{DS})}{\partial V_{GS}} \right]^{-1}. \quad (5)$$

The magnitude of bias voltage is indicated in the equation. It is needed when increasing tenfold current in sub-threshold region. To summarize, this is an ability to control the on/off of gate channel. The smaller this parameter is, the better the efficiency of device is.

The above-mentioned parameters are different between STD (untreated pentacene-based)-OTFT and UV-OTFT, as shown in Fig. 3. The least change under four conditions is the S.S. transforms in the figure. Threshold voltage shift (V_{th}) and sub-threshold slope of STD-OTFT and UV-OTFT are steady in nitrogen environment in addition to the variation of turn-on current (I_d/I_{d0}) and intrinsic mobility (μ/μ_0). In ammonia surrounding, the I_d/I_{d0}, ΔV_{th}, and μ/μ_0 change obviously. Threshold voltage shift has contributed to more obvious changes in

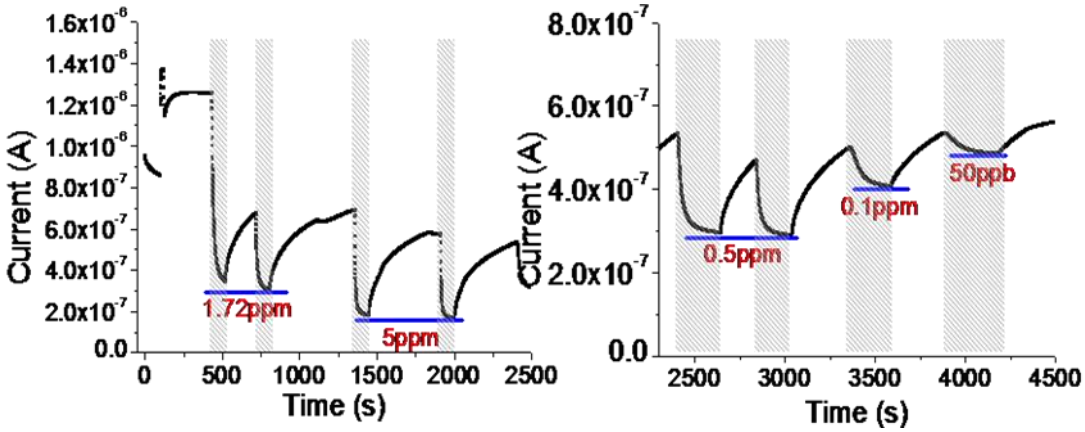

Fig. 4. The drain current versus time for several ammonia concentrations in nitrogen environment [18].

sensing behavior comparing the other three factors. In contrast between STD-OTFT and UV-OTFT, the high efficiency is easy to perceive. Because of increasing dipole moment of PMMA end-groups by UV-light irradiates PMMA, the results indicate that promoting interaction between ammonia molecules and surface of OTFT.

2.2.2 Preconditions and Experiment Results

Other electric characterizations are revealed and demonstrate better sense response because of the ΔV_{th} factor. They can be used well, for example current is experimented on some preconditions.

Ammonia is sensed by OTFT in linear region in this case. According to Eq. (1), when the voltage is biased fixedly on gate-source and drain-source, the drain current varies according to ΔV_{th}. Because of Eq. (2), the variation of the drain current is proportional to ΔV_{th} when overdrive voltage is higher than drain-source voltage. As previously mentioned, the concentration of ammonia is closely related to the ΔV_{th}. Thus this study can extrapolate the positive correlation between the concentration of ammonia and the drain current at present. Fig. 4 shows the drain current versus time for several ammonia concentrations individually in nitrogen environments. The ammonia sensing responses in nitrogen environment is revealed in the figure.

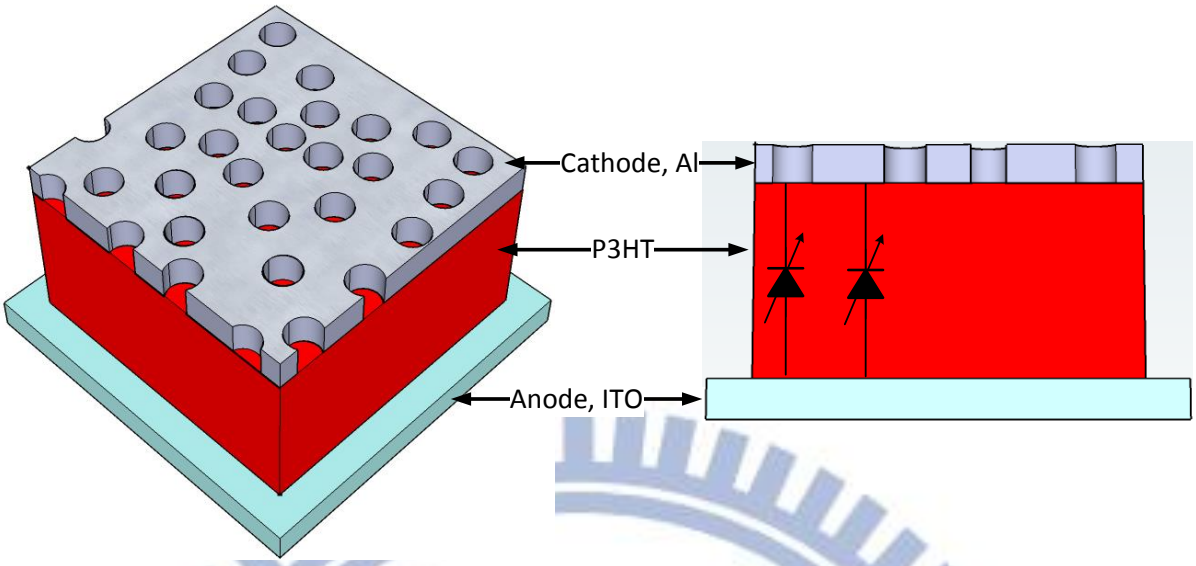

Fig. 5. The structure of VNJ-P3HT diode [19].

2.3 Characteristics of VNJ-P3HT Diode

Only the concentration of ammonia larger than 100ppb can be detected by the Pentacene-based OTFT. A sensing system with high selectivity and the lowest detection lower than 50 ppb is required to detect the breath ammonia.

2.3.1 Structure of VNJ-P3HT Diode

In previous chapters, the structure of the Pentacene-based OTFT is complex. Analyzing by analog IC or other portable devices is difficult because the output current of the Pentacene-based OTFT is small, as shown in Fig. 4. Thus an organic diode with vertical nano-junctions (VNJ) produced by using low-cost colloidal lithography is developed [19]. The lowest detection lower than 20 ppb, real-time response, good enough selectivity, simple structure, high reproducibility and low production costs are advantages of the proposed ammonia sensor. Fig. 5 shows the structure of VNJ-P3HT diode. The ammonia sensing layer is made of the P3HT [poly (3-hexylthiophene)]. The aluminum (Al) was used as cathode. High-density nano-pores on the cathode are produced by using the low-cost colloidal lithography to facilitate the interaction between the molecules of gaseous ammonia and P3HT film. The Indium tin oxide (ITO) film was deposited to be anode.

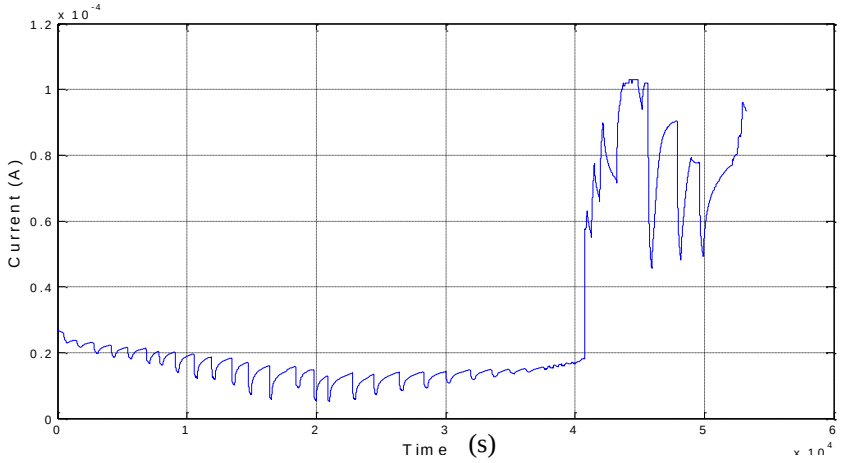

Fig. 6. The output current of VNJ-P3HT diode in 2V bias [19].

2.3.2 Electric Characterization of VNJ-P3HT Diode

Without interacting with ammonia, Fig. 6 shows the output current of the VNJ-P3HT diode when the sensor is biased at 2V. And the output current of the VNJ-P3HT diode is called I_s. Just before interacting with ammonia, the output current of the VNJ-P3HT diode is defined as initial current (I_0). The initial current changes unexpectedly from time to time, as shown in Fig. 6. The range of the initial current is 10μA to 100μA roughly. The output current's values of the VNJ-P3HT diode also change according to variation of the initial current. Thus it's difficult to determine the concentration of ammonia just by the output current's values of the VNJ-P3HT diode when initial current changes from time to time.

2.4 Ammonia Sensing Responses of VNJ-P3HT Diode

2.4.1 Primary Parameters of VNJ-P3HT Diode

Ammonia molecules react with these VNJ-P3HT diodes by diffusing into the P3HT film through the high-density pores, dedoping the P3HT film, and reducing the diode's current. The more ammonia is absorbed by sensor, the less current of output is produced. The value of current doesn't change anymore until the current saturates. The current in steady state is called saturation current (I_{ss}). Finally, the different specific gas concentration can be presented

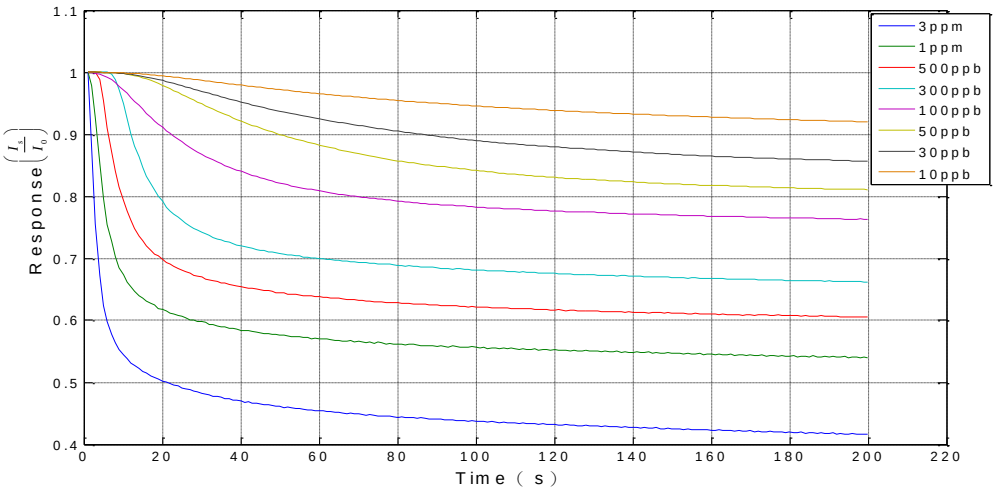

Fig. 7. The original data of response ($\frac{I_s}{I_0}$) in 10ppb ~ 3ppm of ammonia [19].

by the ratio of saturation current to initial current ($\frac{I_{ss}}{I_0}$). This study defines a response as the ratio of the VNJ-P3HT diode's output current to the initial current ($\frac{I_s}{I_0}$).

2.4.2 Preconditions and Experiment Results

The responses in 10ppb ~ 3ppm of ammonia are shown in Fig. 7. The output current of the VNJ-P3HT diode doesn't change anymore because the responses are saturated after 200 seconds. The time of the initial current's unexpected change from time to time is much longer than 200 seconds (as Fig. 6) and therefore it can be ignored. Thus the concentration of ammonia can be determined by the responses in steady state (saturation).

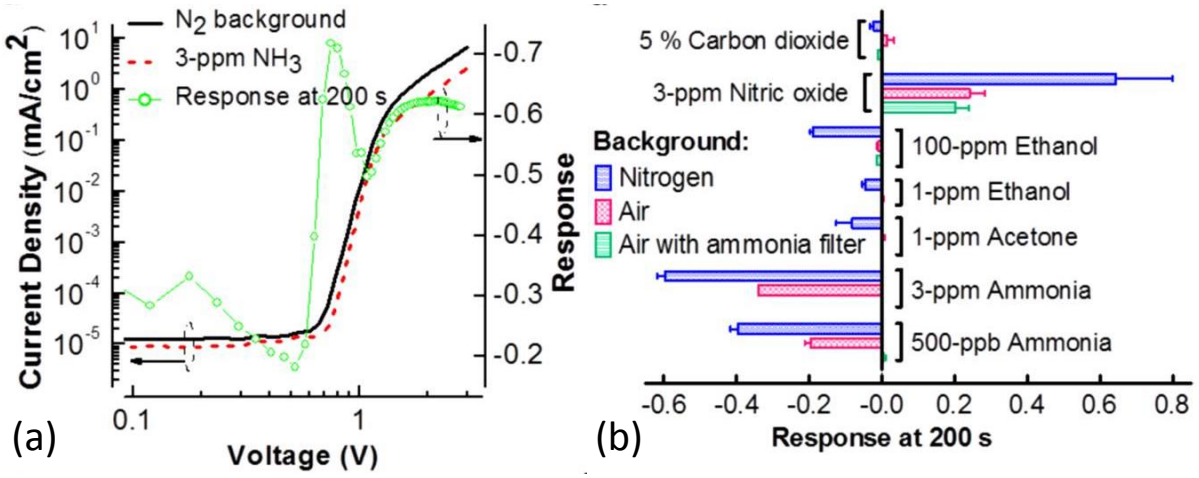

Fig. 8. (a) J−V curve of VNJ-P3HT diodes before (black solid curve) and after 200 s of 3 ppm ammonia sensing (red dashed curve). Green symbols represent the response (i.e., the current variation ratio) of VNJ-P3HT diodes. (b) The responses (measured at 2 V with a fixed sensing time as 200 s) to carbon dioxide (5%), nitric oxide (3 ppm), ethanol (100 and 1 ppm), acetone (1 ppm), and ammonia (3 ppm and 500 ppb). Blue bars, red bars, and green bars represent responses with backgrounds as pure nitrogen, dry air, and dry air passing through commercial ammonia filter ($NiCl_2 \cdot 6H_2O$ powders) [19].

Fig. 8(a) shows the current density as a function of applied bias voltage (J−V curves) of the VNJ-P3HT diode. The current density is proportional to the square of the applied bias voltage, indicating that the holes in P3HT follow the space-charge-limited conduction (SCLC). That is to say, the carrier transport in most intrinsic or low-doped conjugated polymers follows the space-charge-limited current. Thus the injected charge carrier density is much higher than the background doping density in most volume of the sample (i.e., in the bulk region). Because the injected charges are unipolar carriers with very low mobility, they are considered as space charges. Finally, the injected charges are closer to the injection interface have a higher charge density.

The J − V curve of the VNJ-P3HT diode is shown by the red dashed line in Fig. 8(a) after injecting the 3 ppm ammonia (with a background of nitrogen) for 200 s. After contact with ammonia, the slightly right shift of the onset voltage indicates a slight increase of hole injection barrier. However, the main reaction is the current decline in the SCLC zone. The

ratio of saturation current to initial current ($\frac{I_{ss}}{I_0}$) is used to represent the response of the sensor. The green symbols in Fig. 8(a) shows the response to the 3ppm ammonia 200 seconds exposure plotted as a function of applied bias. The peak of response is at around 0.8 V. But the current of diode at 0.8 V is too low to provide a good signal-to-noise ratio. A large and stable response as −0.6 is obtained when the applied bias voltage changes from 1.5 to 3 V. Thus this study chooses 2 V as a fixed applied bias voltage to measure the response in the following works.

The relations are all the same in different concentration of ammonia according to [19]. The responses in steady state are same, which can determine the concentration of ammonia when the VNJ-P3HT diode is biased in 1.5~3V. Thus this study chooses the VNJ-P3HT diode as the sensor device at present. If this study tries to operate the diode sensor accurately, it needs to satisfy:

1. 1.5~3V should be applied to the bias of the sensor.
2. When initial current varies from 10~100μA, this study can perform response.
3. In order to present the specific gas concentration, use response in steady state.
4. 10ppb of ammonia can be detected by the sensor.

The responses of the VNJ-P3HT diode are also analyzed to several kinds of gases existing in human respiratory gas. The responses of the VNJ-P3HT diode (measured at 2 V with a fixed sensing time as 200 seconds) to carbon dioxide (5%), nitric oxide (3 ppm), ethanol (100 and 1 ppm), acetone (1 ppm) and ammonia (3 ppm and 500 ppb) are compared in Fig. 8(b). The responses with backgrounds as pure nitrogen, dry air, and dry air passing through commercial ammonia filter (NiCl2•6H2O powders) are represented by blue bars, red bars and green bars. Because of the greatly suppressed vapor pressure of ethanol (2 mmHg) and acetone (20 mmHg) at −20 °C, the response to ethanol and acetone in dry air are significantly suppressed. Thus the VNJ-P3HT diode has very small responses (0.009 to

−0.017) to ethanol and acetone with dry air as the background. That is to say, cooling the tube at −20 °C before connecting to the sensor device (i.e., the sensor is at room temperature) leads to a suppressed humidity and suppressed concentrations of VOCs. The concentration of ammonia should not be significantly changed in our system because the boiling point of ammonia is −33.3 °C. On the other hand, the response to 3 ppm nitric oxide is positive and significant. Because of the oxidation (doping) of P3HT, the reaction is known and irreversible. Fortunately, the concentration of nitric oxide is very low in our breath (<40 ppb).

The responses of a fresh VNJ-P3HT diode and of a 5 hours aged VNJ-P3HT diode to 400 ppb ammonia as a function of time are compared in breath ammonia testing. The aged sample was used to detect breath ammonia of rats for 12 times during 5 hours. The difference between response of the fresh sample and response of the aged sample is within 4% proving that the VNJ-P3HT diode is reliable enough for at least 5 hours of operation.

CHAPTER 3

The Novel Sensing Circuit for Organic Gas Sensors

The instruments are usually used to measure the gas concentration sensed by VNJ-P3HT diode. There are few chip design studies which focus on the back-end read-out circuit because of the property of sensor device. The design of the proposed sensing circuit can provide more benefits for real-time detection of gas concentration compared with the measurement by traditional instruments. In order to detect ammonia concentration based on steady state current, the responses of VNJ-P3HT diode are measured. This study designs the sensing circuit to process current variation of VNJ-P3HT diode for varied ammonia concentrations. Because of using the ratio of saturation current to initial current to determining ammonia concentration, the sensing circuit solves the problem that the initial current of VNJ-P3HT diode are different from time to time. The real-time detection and convenient for diagnosis can also be achieved by the sensing circuit for biomedical usages. A readout circuit is needed to design as interface with the VNJ-P3HT diode at first. The output voltage which is converted by the output current of front-end sensors through the principle of a trans-impedance amplifier (TIA) can be processed by this circuit. The linear or other relationships between output signals of sensor circuit and gas concentration must be achieved in the next step. It is stand for that the gas concentration can be directly detected by output signals from back-end circuit. Thus the accurate and convenient medical measurement can be further achieved.

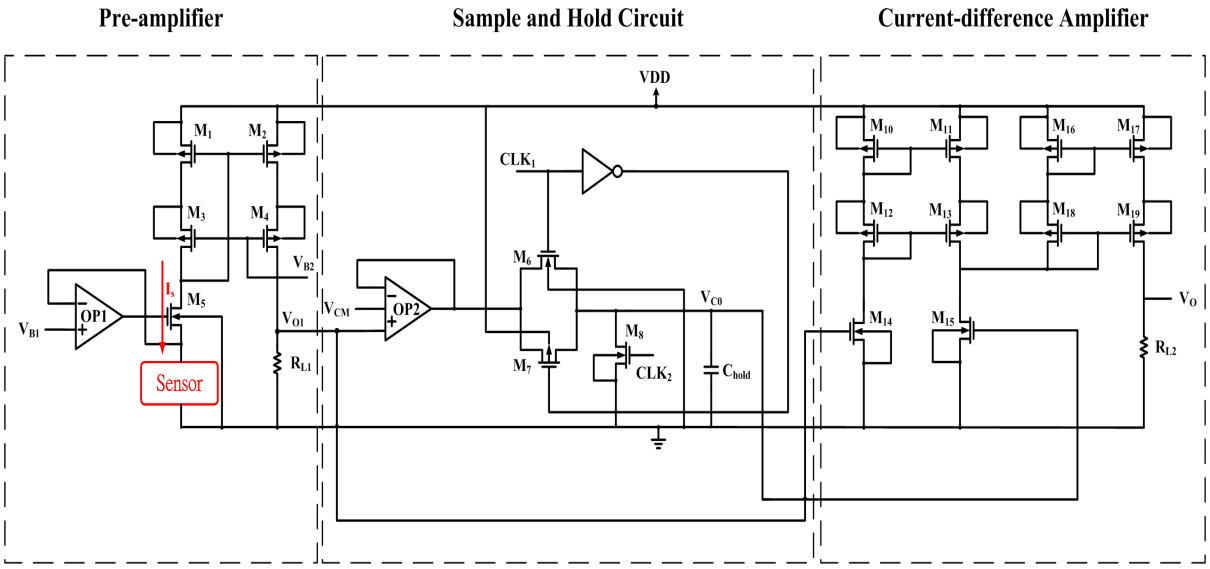

Fig. 9. Readout circuit for OTFT sensor [20].

3.1 Review of Past Sensing Circuits

3.1.1 A Readout Circuit for an OTFT Gas Sensor with a New Preamplifier

Fig. 9 shows that the previous readout circuit consists of a pre-amplifier, a sample and hold circuit and a differential current amplifier [20]. In order to convert the output current of a gas sensor into voltage, a pre-amplifier is composed of trans-impedance. According to distinct designing time instants in a target gas environment, the sample and hold circuit memorizes various voltages. The differential current is attributable to the voltages of sample and hold circuit using current mirror framework. Then a differential current amplifier amplifies the differential current. The differential current is converted into output voltage through the resistance load. In order to determine gas concentration database of pre-measured which are contrast, a micro-processor control unit (MCU) acquires and stores the outputs.

There are two major disadvantages in the previous readout circuit. First, the voltage value is recorded by a capacitor C_{hold} of the sample and hold circuit. The voltage drop problem is serious because of the leakage current of the capacitor. Second, the value of initial

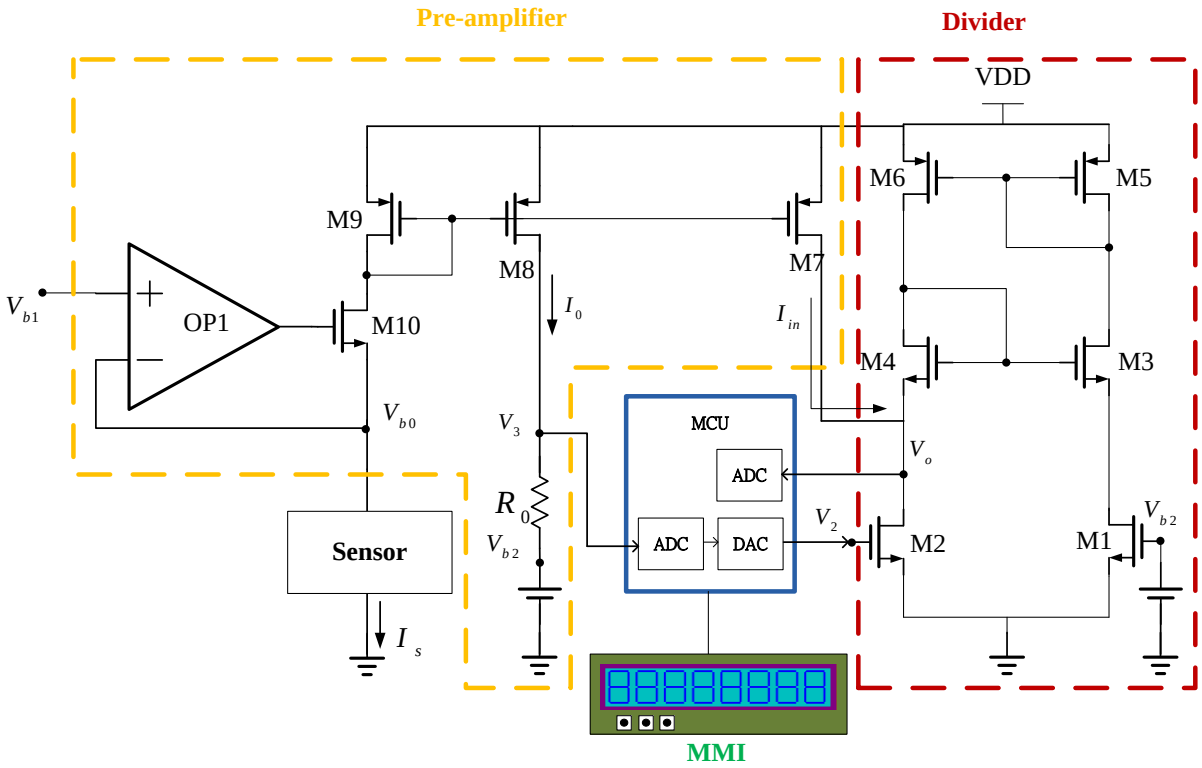

Fig. 10. The sensing system for OTFT sensor [21].

current changes unexpectedly from time to time in the previous chapter. But the design of previous sensing circuit is based on stable OTFT sensors, which means that the initial current of OTFT sensors doesn't change from time to time. The output of the differential current amplifier changes and the gas concentration database is unreliable when the value of initial current changes.

3.1.2 A Front-end Readout Circuit Including an Analog Divider for an OTFT Gas Sensor

The previous readout system (shown in Fig. 10) consists of an analog IC, a micro-processor control unit (MCU) and Man-Machine Interface (MMI). The analog IC comprises further a pre-amplifier and an analog divider, which are used to be an interface with the OTFTs sensors and calculate the ratio of saturation current to initial current. The CPU of proposed MCU is LPC1768 by NXP. The AD/DA of MCU holds the input value of the analog divider and the

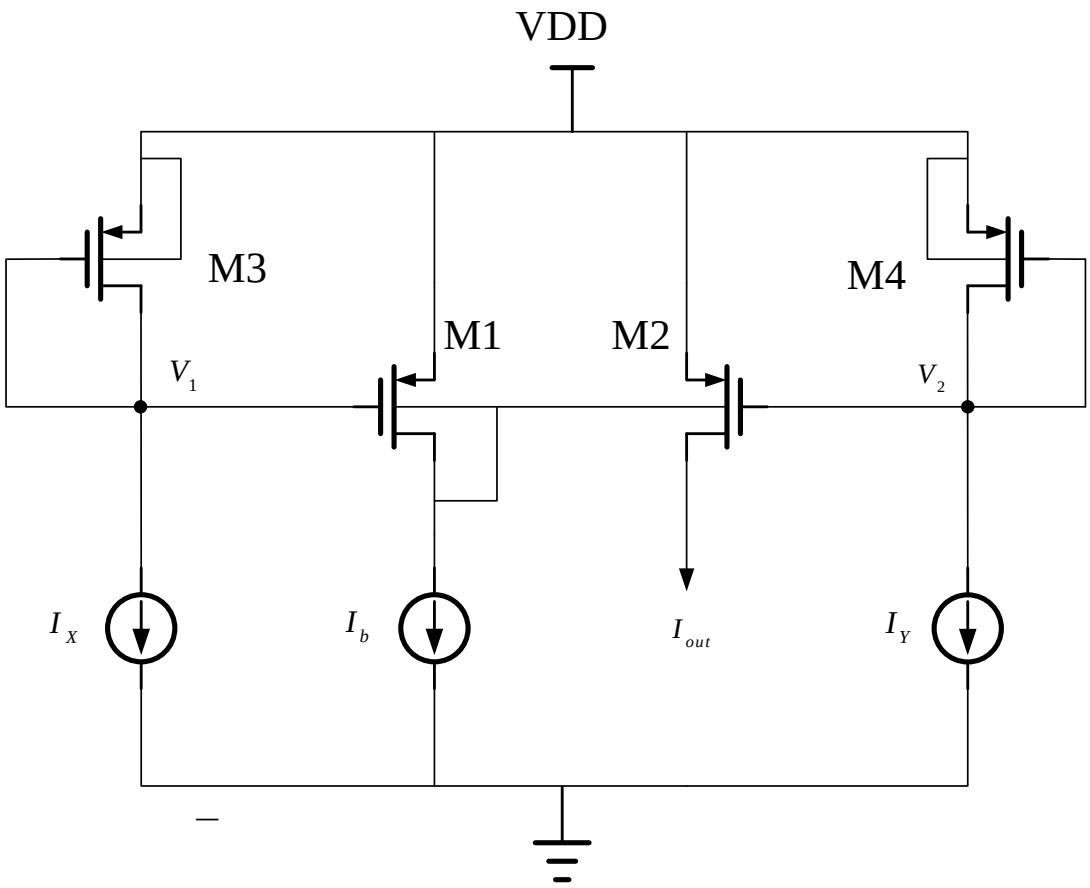

Fig. 11. Weak inversion divider circuit [22].

ADC of MCU is used to calculate and store the output data of readout circuit. The MMI comprises further a Liquid Crystal Display (LCD) module and buttons. It is applied to be conveniently used by users and displays results of sensing system, which is controlled by the MCU.

The previous readout circuit also shows two major disadvantages. First, the system includes a MCU and an analog circuit, causing complexity to increase. Second, the design is not accurate, because it is limited by the resolution of the AD/DA converter.

3.2 Types of Divider Circuit

The analog signal processing circuits use the analog divider circuit widely, for example the filters, hearing-aid systems and logarithmic function generators. According to different circuit principles, many types of analog dividers are designed.

3.2.1 Weak Inversion Divider

The divider and 1/x functions can be performed by a CMOS current-mode circuit in this study. In order to meet the application of division, the design uses MOSFETs biased in weak inversion. Fig. 11 shows the proposed circuit. The drain current of a PMOS transistor in weak inversion is given by

$$I_D = I_{DO} \exp\left(\frac{V_{SG} + (n-1)V_{SB}}{nU_T}\right), \tag{6}$$

where I_{DO} is the leakage current, n is the slope factor and U_T (=kT/q) is the thermal voltage. The output current in Fig. 11 is given by

$$I_D = I_b \exp\left(\frac{V_1 - V_2}{nU_T}\right). \tag{7}$$

V_1 and V_2 can be formed in logarithm as

$$V_1 = V_{DD} - nU_T \ln\left(\frac{I_X}{I_{D0}}\right) \tag{8}$$

and

$$V_2 = V_{DD} - nU_T \ln\left(\frac{I_Y}{I_{D0}}\right). \tag{9}$$

Combining Eq. (4), (5) and (6), the output current I_{out} is given by

$$I_{out} = I_b \frac{I_Y}{I_X}. \tag{10}$$

Eq. (10) implements a current-mode divider circuit when the bias current I_b keep constant. The input current (I_X, I_Y) and output current (I_{OUT}) are too small to be used for organic gas sensor because the MOSFETs are biased in weak inversion. The minimum output current of organic gas sensor is at least greater than 10 μA.

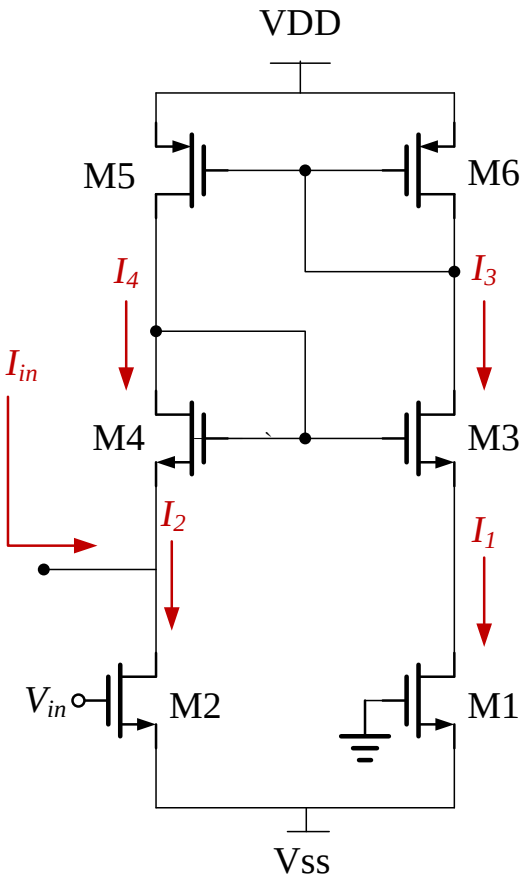

Fig. 12. Divider circuit for organic sensor [23].

3.2.2 Current-to-Voltage Mode Divider

Fig. 12 shows the proposed circuit. If both M1 and M2 are biased in the triode region without body effect, the source currents I_1 and I_2 can be expressed as

$$I_1 = \frac{K_{n1}}{2}(2(-V_{SS} - V_{Tn1})V_{DS1} - V_{DS1}^2) \tag{11}$$

and

$$I_2 = I_{in} + I_4 = \frac{K_{n2}}{2}(2(V_{in} - V_{SS} - V_{Tn2})V_{DS2} - V_{DS2}^2), \tag{12}$$

where I_{in} is input current, $K_{n1,2}$ are the trans-conductance parameters and $V_{Tn1,2}$ are the threshold voltages of M1 and M2, respectively. The current mirror, M5 and M6, is used to copy the current I_1, so that

$$I_1 = I_3 = I_4 . \tag{13}$$

The source voltages of M3 and M4 are equal ($V_{SB3} = V_{SB4}$ so $V_{Tn3} = V_{Tn4}$) and both of them are biased in saturation if they are matched ($K_{n3} = K_{n4}$). Because of the square-law characteristics of MOSFETs, the equation can be found as

$$V_{GS3} = V_{GS4} = \sqrt{\frac{2I_1}{K_{n3}}} + V_{Tn3} . \tag{14}$$

According to $V_{GS3} + V_{DS1} = V_{GS4} + V_{DS2}$ and Eq. (13), (14) ,it can have

$$V_{DS1} = V_{DS2} . \tag{15}$$

Assuming that M1 and M2 are matched ($K_{n1} = K_{n2} = K_n$ and $V_{Tn1} = V_{Tn2} = V_{Tn}$) and substituting Eq. (11), (13) and (15) into Eq. (12), it can have

$$V_{DS2} = \frac{I_{in}}{K_n V_{in}} . \tag{16}$$

A current-to-voltage-mode divider circuit is implemented in Eq. (16). The input current (I_{in}) can be up to 100 μA because the M1 and M2 biased in the triode region. Thus the current-to-voltage-mode divider can be used for OTFT gas sensor.

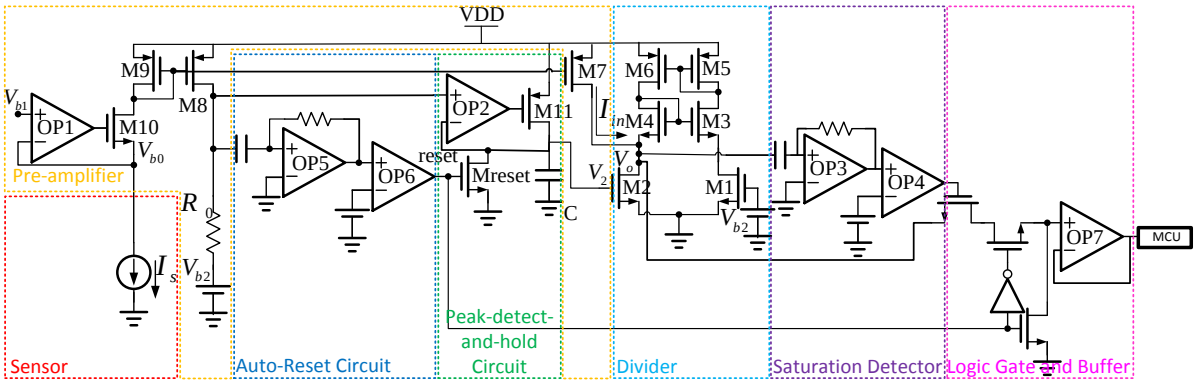

Fig. 13. The readout circuit for VNJ-P3HT diode.

3.3 The Sensing Circuit for Organic Gas Sensors

Fig. 13 illustrates the entire readout circuit. It can be seen that the circuit consists of six parts, a pre-amplifier, a peak-detect-and-hold circuit, a divider, a saturation detector, an auto-reset circuit and a result-or-zero circuit. The six parts are designed on-chip, which is accomplished by Taiwan Semiconductor Manufacturing Company (TSMC) 0.35μm 2P4M 3.3V mixed-signal CMOS process.

The VNJ-P3HT diode sensor component is represented by a block of sensor. The sensed current that reflects the concentration of sensed gas that interacts with surface on the VNJ-P3HT diode is denoted by I_s. Ammonia is chose as the gas to sense in our study. The operation principle of the VNJ-P3HT diode is based on the change of initial current from time to time mentioned in the previous chapter. Compared to the time that initial current change, which can be ignored, the sensing time is 200 seconds, which is very fast. The more ammonia is absorbed by the surface of the VNJ-P3HT diode, the less current of output is produced. The ratio of saturation current to initial current can present the specific gas concentration according to previous chapter. The readout circuit must records the value of initial current to calculate the ratio of saturation current to initial current. As a result, the pre-amplifier is intended in acquire the initial current information in voltage signals and pays the way for the design of a current-to-voltage converter (a trans-impedance converter) in the following. In the

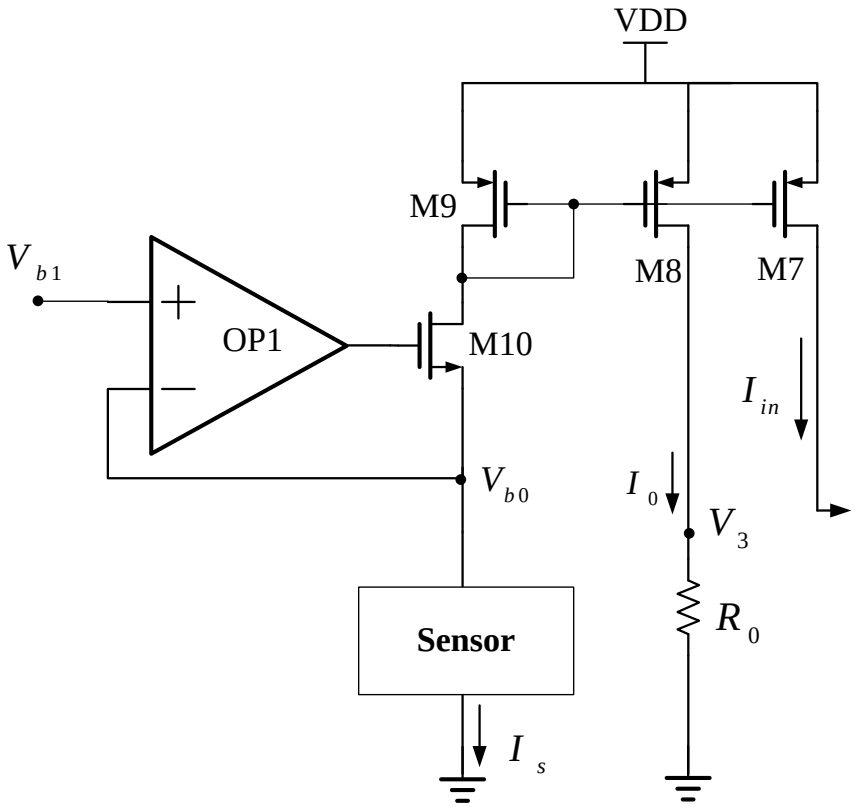

Fig. 14. Pre-amplifier.

previous design, the MCU is used to record the voltage value. Due to adding of MCU, the incremental complexity is serious and the design is not accurate. As result, the peak-detect-and-hold circuit and super capacitor are used. The system integration between the analog IC and MCU can be accomplished, become a chip. Compared to previous current difference amplifier, the current-to-voltage-mode divider circuit can calculate the value of input current divided by input voltage. The input voltage is provided by the output of peak-detect-and-hold circuit and the input current is provided by the current mirror (M9-7). With the Auto-Reset circuit, saturation detector and logic gate, the circuit achieves an automatic easy-to-use readout circuit. The MCU records the output value of analog divider and transforms it into gas concentration. The LCD shows the value of gas concentration.

3.3.1 Pre-Amplifier

Fig. 14 shows that the pre-amplifier comprises further two current copiers (M9-8 and M9-7),

a set of clamped op (OP1) and a negative feedback NMOS transistor [24]. The voltage across the VNJ-P3HT diode sensor V_{b0} is able to be approximately fixed to V_{b1} because of the negative feedback OP1 with the output connected to the gate voltage of M10. V_{b1} can control the bias voltage of VNJ-P3HT diode sensor. The advantage of this circuit structure is that can ignore the output impedance of the sensor. The only acquired information is the experiment data from sensor component. The reason for analyzing equivalent circuit of sensor is the shortage of completed information for parametric analysis and modeling sensor component. The gate voltage of the transistor M10 is regulated to achieve balance of the negative feedback circuit. When MOSFET operate in saturation, slight variation of gate voltage can control a great quantity of drain current. The drain current has a great acceptance region with least output swing range of OP1 depending on adjusting gate voltage. And in the meanwhile biasing sensor component and ensuring OP1 work in normal region do not affect current path for sensed current only flows through M10. The output current of the VNJ-P3HT diode is inversely proportional to the concentration of the sensed gas and steadily in this way. The two current mirrors (M9-8 and M9-7) next copy the current of VNJ-P3HT diode. This study uses the current mirror (M9-8) to transform initial current (I_0) into voltage by resistance R_0. Consequently, the initial current information ($I_0 R_0$) is recorded by super capacitor of the peak-detect-and-hold circuit. Meanwhile, this study uses the other current mirror (M9-7) to copy the I_s as I_{in}, which is input current of the analog divider.

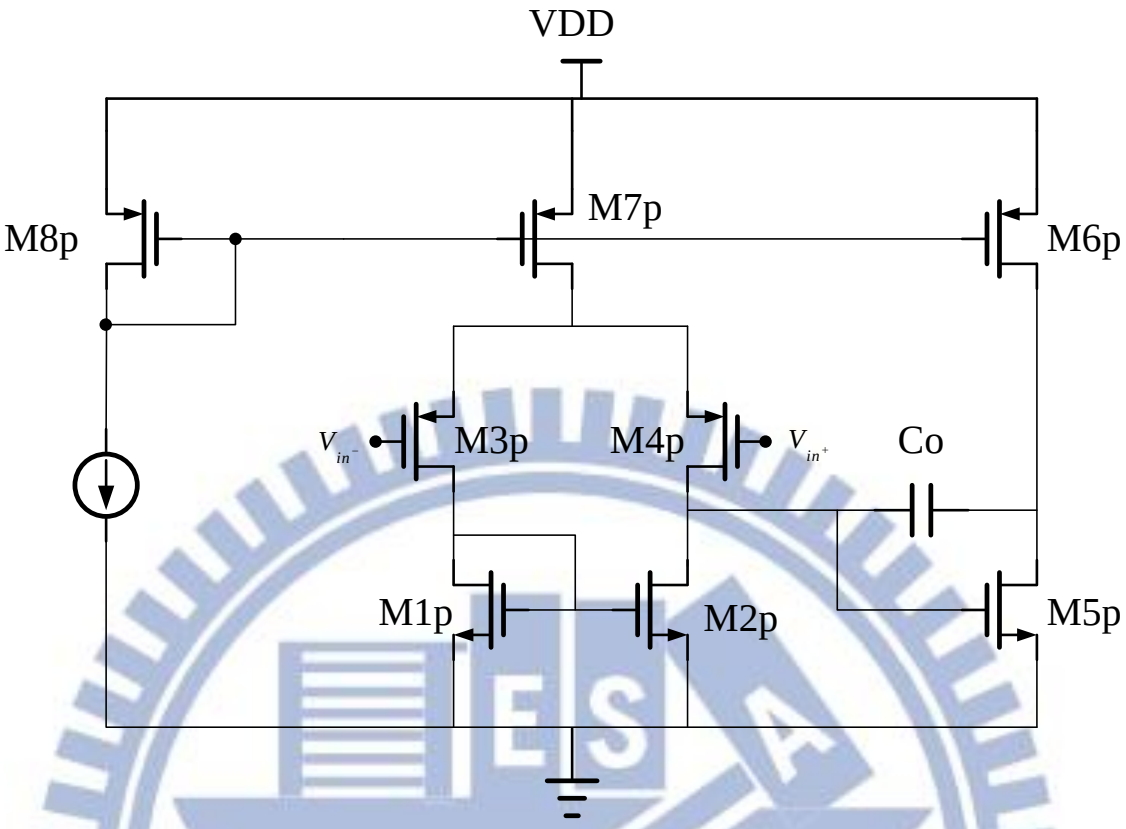

Fig. 15. Two-stage operation amplifier.

In the first and second stages of Fig. 15, the active current mirrors are used as loads for differential pairs and are also gain stages of this amplifier. The gain of the two-stage amplifier is above 70dB.

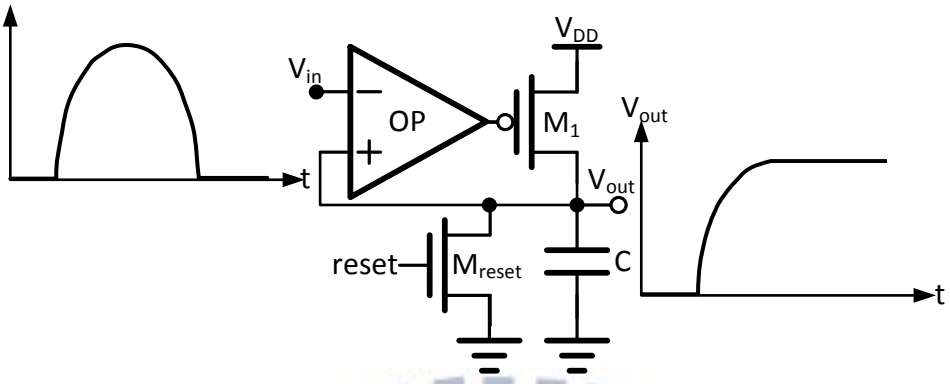

Fig. 16. Peak-detector-and-hold (PDH) circuit.

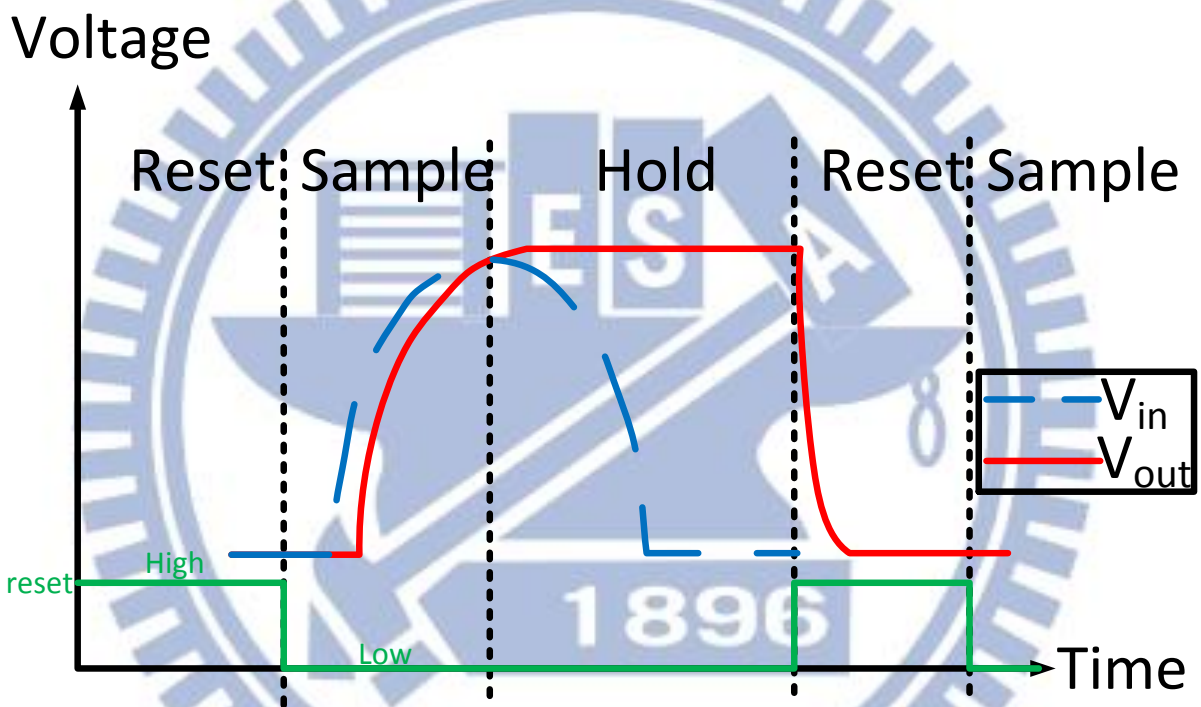

Fig. 17. PDH timing diagram of operations.

3.3.2 Peak-Detect-and-Hold Circuit

The peak-detector-and-hold (PDH) circuit is shown in Fig. 16 with the timing diagram of operations in Fig. 17. One cycle of operation consists of three phases including Reset, Sample and Hold time intervals. In the reset phase, the control signal “reset” is a high voltage level “1” to enable the capacitance “C” discharged to ground voltage. During the sample phase, the control signal reset is a low voltage level “0”. When the input voltage Vin is greater than the

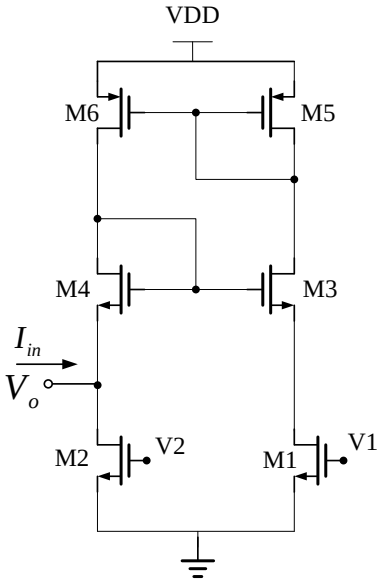

Fig. 18. Current-to-voltage-mode divider circuit [23].

output voltage Vout, the output of the amplifier is a low voltage level "0", the PMOS M1 is turned on and the capacitance C is charged until the input voltage is equal to Vout. When Vin is smaller than the output voltage, the amplifier's output is "1" and M1 turns off. The output voltage Vout is so sustained as the maximum value of input voltage until the next reset phase begins. When sensor device starts to react with gas, the output current will decrease. The maximum value of input voltage always is the voltage transformed from initial current. Thus this study uses the circuit to acquire the initial current information in voltage signals.

3.3.3 Divider Circuit

A current-to-voltage analog divider can be realized because of Eq. (16). In order to operate the proposed current-to-voltage analog divider with a unipolar supply voltage, it can be further modified, as shown in Fig. 18. The reference voltages V_1 and V_2 are connected to the gates of M_1 and M_2, respectively and the sources of M_1 and M_2 are grounded. From Eq. (11) - (15), Eq. (16) can be modified as

$$V_o = \frac{I_{in}}{K_n(V_2 - V_1)}. \tag{17}$$

A current-to-voltage-mode divider can be realized and its gain can be adjusted by the reference voltages V_1 and V_2 because of Eq. (17). The output offset voltage is not generated by the proposed current-to-voltage analog divider under unipolar supply voltage. The drain voltages of M_1 and M_2 are lower than their gate voltages by a threshold voltage when V_1 and V_2 are biased in triode region. As a result, the proposed circuit works for low supply voltages.

Fig. 13 shows the proposed sensing system, V_1 and V_2 are biased by V_{b2} and $I_0R_0 + V_{b2}$, respectively. It can have

$$V_2 - V_1 = I_0R_0. \tag{18}$$

From Eq. (17), It can have

$$V_o = \frac{I_s}{K_n\left(R_0I_0\right)} = \frac{1}{K_nR_0}\left(\frac{I_s}{I_0}\right). \tag{19}$$

Finally, the ratio of saturation current ($I_{Sensor}^{'}$) to initial current (I_0) multiply by a constant ($\frac{1}{K_nR_0}$) is presented by the output voltage of analog divider, which can present the specific gas concentration when the response is done.

3.3.4 Saturation Detector

Fig. 7 shows that after 200 seconds the responses are saturated cause the output current of the VNJ-diode OTFT doesn't change anymore. The responses in steady state (saturation) can determine the concentration of ammonia. But timing it with a stopwatch is inconvenient. Compared with using the stopwatch, the design of the proposed saturation detector can provide more convenience for real-time detection of gas concentration.

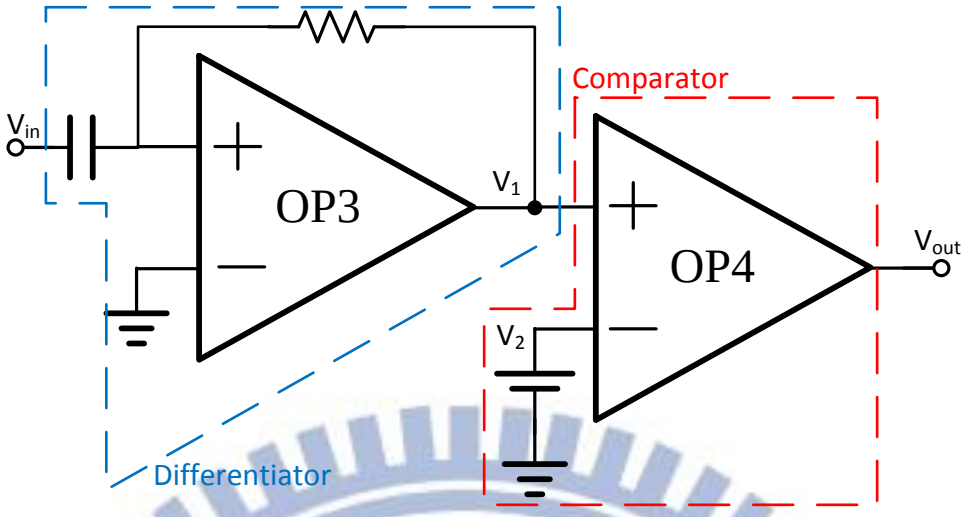

Fig. 19. Saturation detector.

When the response is saturated, the output current of the VNJ-P3HT diode doesn't change anymore. This study can make good use of this characteristic. If the output current of the VNJ-P3HT diode doesn't change anymore, its rate of change is close to zero. After differentiation, the output of the differentiator is also close to zero. So a differentiator and a comparator are used to detect when the response is saturated. The circuit of the saturation detector is shown in Fig. 19.

A differentiator is a circuit that is designed such that the output of the circuit is approximately directly proportional to the rate of change (the time derivative) of the input. A differentiator circuit includes an operational amplifier (shown in Fig.15.), the resistor is used at feedback side and capacitors are used at the input side. The circuit is based on the capacitor's current to voltage relationship,

$$I = C\frac{dV}{dt}, \tag{20}$$

where I is the current through the capacitor, C is the capacitance of the capacitor, and V is the voltage across the capacitor. The current flowing through the capacitor is then proportional to the derivative of the voltage across the capacitor. This current can then be connected to a resistor, which has the current to voltage relationship,

$$I = \frac{V}{R}, \tag{21}$$

where R is the resistance of the resistor. Note that the operational amplifier input has a very high input impedance (which also forms a virtual ground) so that the entire input current has to flow through R. If V1 is the voltage across the resistor and Vin is the voltage across the capacitor, these two equations can be rearranged to obtain the equation,

$$V_1 = RC\frac{dV_{\text{in}}}{dt}. \tag{22}$$

Thus, it can be shown that in an ideal case the voltage across the resistor is proportional to the derivative of the voltage across the capacitor with a gain of RC.

A comparator is a device that compares two voltages or currents and switches its output to indicate which is larger. An operational amplifier (op-amp) has a well-balanced difference input and a very high gain. This parallels the characteristics of comparators and can be substituted in applications with low-performance requirements.

In theory, a standard op-amp operating in open-loop configuration (without negative feedback) may be used as a low-performance comparator. When the non-inverting input (V_1) is at a higher voltage than the inverting input (V_2), the high gain of the op-amp causes the output to saturate at the most positive voltage, which can output. When the non-inverting input (V_1) drops below the inverting input (V_2), the output saturates at the most negative voltage which can output. The op-amp's output voltage is limited by the power supply voltage. An operational amplifier operating in a linear mode with negative feedback, using a balanced, split-voltage power supply, (powered by ± V_S) has its transfer function usually written as

$$V_{out} = A_o(V_1 - V_2). \tag{23}$$

However, this equation may not be applicable to a comparator circuit which is non-linear and operates open-loop (no negative feedback).

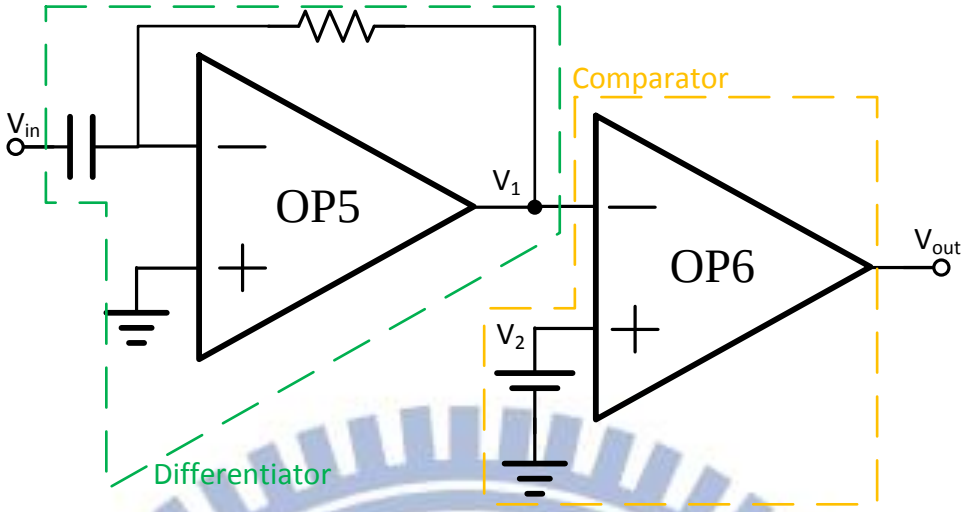

Fig. 20. Auto-reset circuit.

3.3.5 Auto-Reset Circuit

The readout circuit must get a new initial value of the current each time the sensor interact with different concentrations of ammonia. The initial current information in voltage signals is stored in the super capacitor of peak-detector-and-hold circuit (shown in Fig. 16). The users must manually reset the initial current without the Auto-Reset circuit. The proposed Auto-Reset circuit can automatically detect when the sensor device starts to react with gas and reset the voltage value of the peak-detect-and-hold circuit to achieve an automatic readout circuit.

This circuit consists of a differentiator and a comparator, which is shown in Fig. 20. When the VNJ-P3HT diode starts to interact with ammonia, the output current will decrease. The rate of change (the time derivative) of the output current of the sensor is negative at this time. This study can see this phenomenon through a differentiator and reset the initial current information in voltage signals with a comparator.

The auto-reset circuit is similar to the saturation detector except the exchange of the sign of input. Thus the relationship between V_{in} and V_{out} is

$$V_{out} = -RC\frac{dV_{in}}{dt}. \tag{24}$$

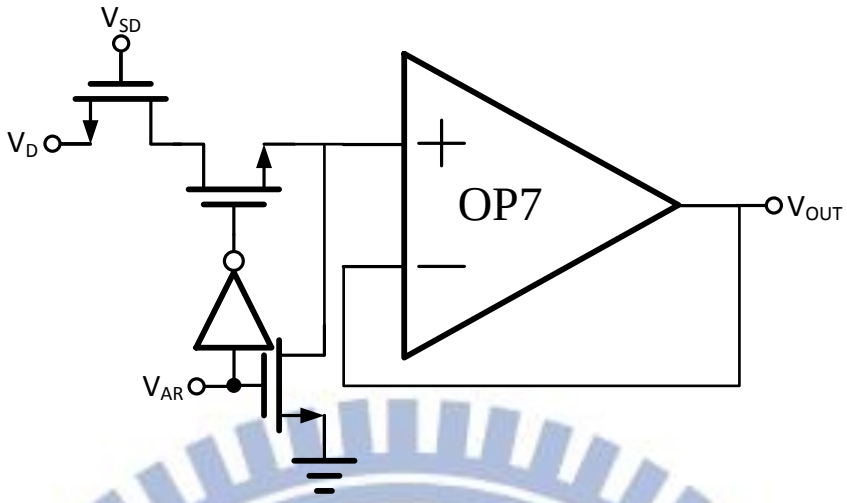

Fig. 21. Logic gate and buffer.

The minus sign indicates the phase difference of 180 degrees between the output and the input.

3.3.6 Logic Gate and Buffer

The output of divider are useless before the current saturate. The logic gate is designed to filter unwanted messages, which is shown in Fig. 21. The output show the result only when sensor react with gas and the current saturate, otherwise the output display zero. The true table is shown in Table I. The circuit allow users to easily read the concentration.

Table I. True table of logic gate.

V_{SD}	V_{AR}	V_{OUT}
0	0	0
0	1	0
1	0	1
1	1	0

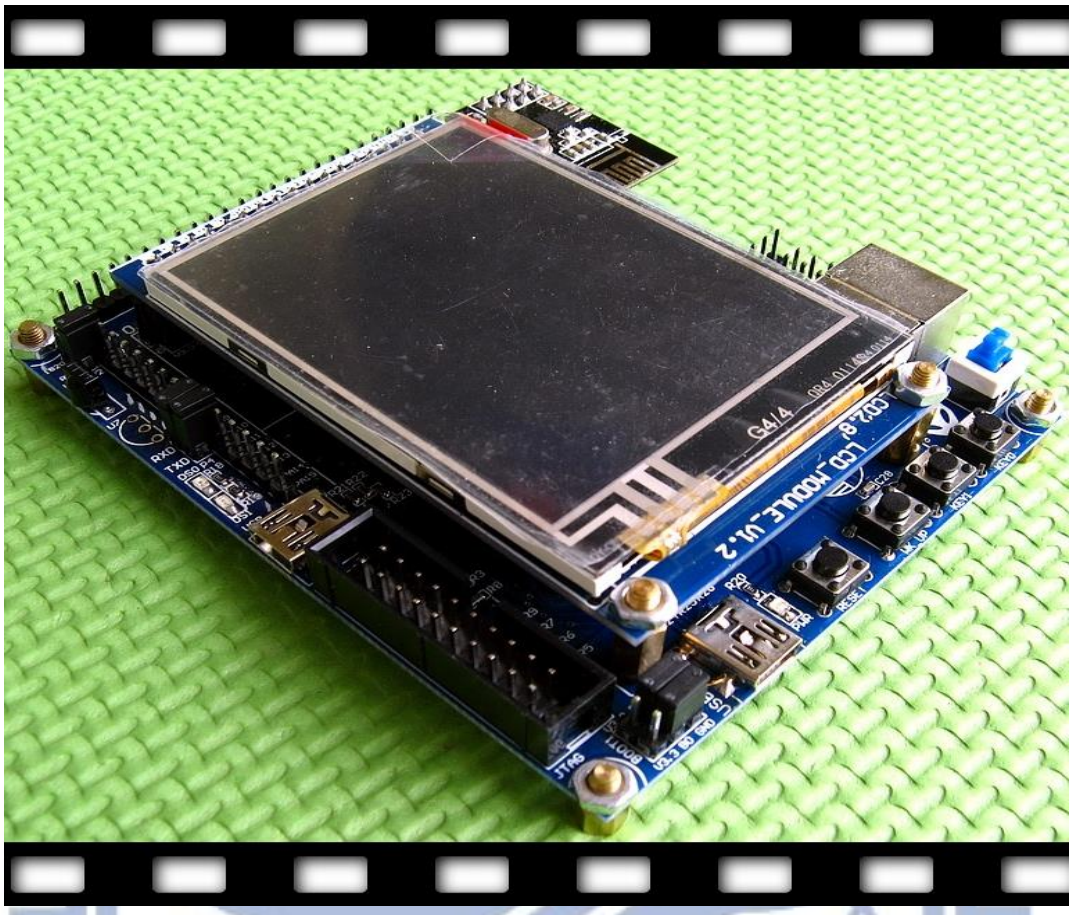

Fig. 22. Micro controller unit.

3.3.7 Micro Controller Unit

STM32 is the Central Processing Unit (CPU) of proposed Micro Controller Unit (MCU) (shown in Fig. 22) by ALIENTEK. It is a micro-controller based on ARM Cortex ™-M processor for embedded applications requiring high performance, real-time capabilities, digital signal processing, and low‑power, low‑voltage operation, while maintaining full integration and ease of development. Its size is only 8cm × 10cm. The peripheral complement of the STM32 includes up to 20kB of SRAM, up to 128kB of FLASH, three 16-bit ordinary timers, a 16-bit high-timer, two SPI, two IIC, three serial ports, a USB interface, a CAN channel, two 12-bit ADC and up to 51 general purpose I/O pins, etc [25]. An ADC, 2.8 inch LCD and 3.3V power supply are required for the sensing system. The maximum conversion rate of ADC is 1 MHz and the input range is 0V~3.3V.

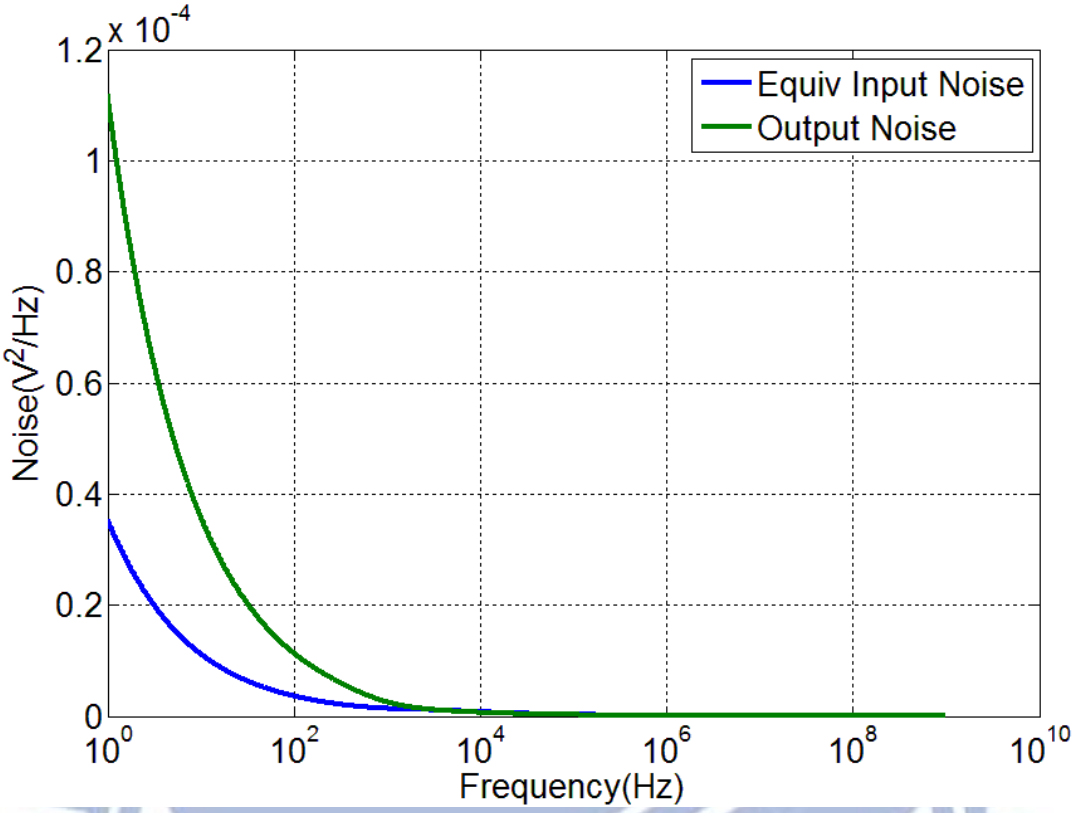

Fig. 23. Output and equivalent input noise.

3.3.8Design Procedure for Sizing all MOSes

Minimizing circuit noise in high resolution readout circuit is critical. Because our circuit operates at low frequency, the flicker noise must be considered. It is better to increase both the length and width of the device, so that the flicker noise comes down. But the noise reduction by increasing device dimensions comes at the cost of area and power consumption. Power consumption is an important factor in portable sensing system design. Thus the power consumption and noise of the circuit were computed using HSPICE corners simulations. Fig. 23 shows the simulations of noise through HSPICE. According to the simulation results, a range of W / L values is shown. These values are quite tolerant to the effects of fabrication errors. An important cost measure for on-chip system is occupied area. The condition is also added in verification process for area in order to combine high quality and low cost for our

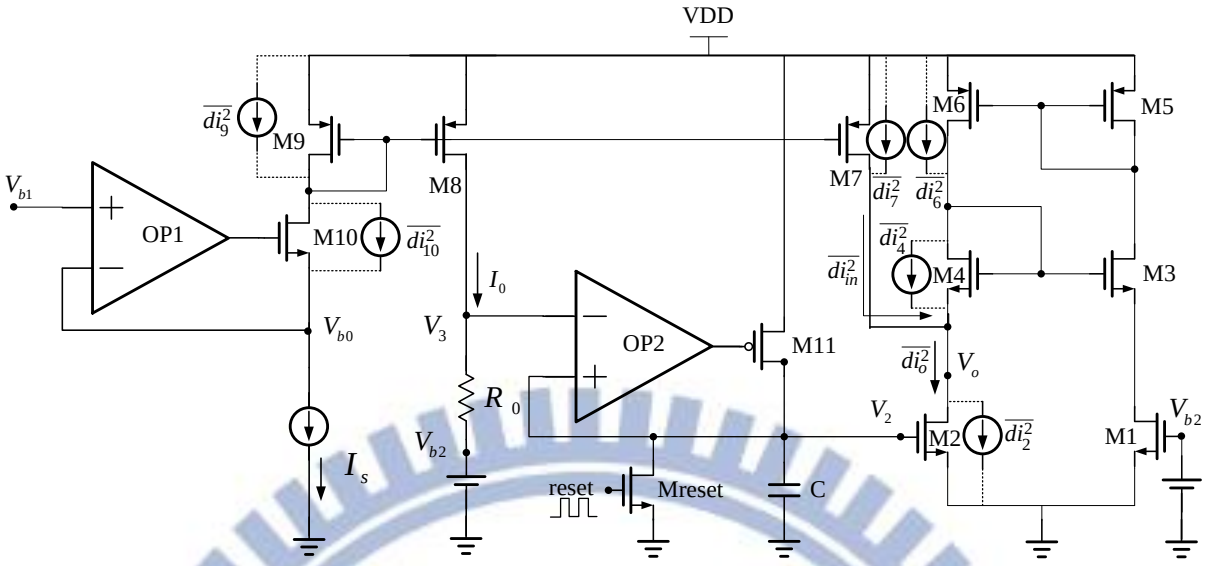

Fig. 24. Noise of readout circuit.

users. Finally, sizing all MOSes leads to a tradeoff between noise, power and area in our study. The readout circuit is successfully achieving a balance between noise, power and area.

3.3.9 Circuit noise analysis

A general noise model for the output of readout circuit is shown in Fig. 24. The noise contributed by each of the transistors can be described by a noise current source $\overline{di_n^2}$ for transistor M_n between the drain and source. Considering only the thermal noise we have

$$\overline{di_{in}^2} = \overline{di_7^2} + 1^2(\overline{di_9^2} + \overline{di_{10}^2}) = \frac{2}{3}4kT(g_{m7} + g_{m9} + g_{m10})df\ , \qquad (25)$$

where $\overline{di_{in}^2}$ is the noise of the current mirror and g_{mn} is the trans-conductance of transistor M_n. With this transistor noise model we find the equivalent output noise current for the readout circuit,

$$\overline{di_o^2} = \overline{di_{in}^2} + \overline{di_6^2} + \overline{di_4^2} + \overline{di_2^2} = \frac{2}{3}4kT(g_{m7} + g_{m9} + g_{m10} + g_{m6} + g_{m4} + g_{m2})df\ . \qquad (26)$$

Obviously, reducing g_m will reduce the thermal noise. Since g_m is proportional to the ratio of width to length $(\frac{W}{L})$, low thermal noise has dictated lower $(\frac{W}{L})$ ratio. We also model the flicker noise of readout circuit by a current source,

$$\overline{I_{o,1/f}^2} = \frac{1}{C_{ox} f}[\frac{g_{m7}^2 K_P}{(WL)_7} + \frac{g_{m6}^2 K_P}{(WL)_6} + \frac{g_{m4}^2 K_N}{(WL)_4} + \frac{g_{m2}^2 K_N}{(WL)_2}]. \quad (27)$$

The output flicker noise voltage per unit bandwidth is therefore equal to

$$\overline{V_{o,1/f}^2} = \frac{1}{C_{ox} f}[\frac{g_{m7}^2 K_P}{(WL)_7} + \frac{g_{m6}^2 K_P}{(WL)_6} + \frac{g_{m4}^2 K_N}{(WL)_4} + \frac{g_{m2}^2 K_N}{(WL)_2}][r_{o7} // (r_{o6} + r_{o4}) // r_{o2}]^2 . \quad (28)$$

Evidently, large widths and lengths will drop the flicker noise down. But larger widths by themselves do not help because the g_m scales up the same amount that the noise goes down. Thus we try to lower the g_m so that the flicker voltage at the gate produces less current at the drain.

CHAPTER 4

Simulations and Experimental Results

4.1 Simulation of the Designed Sensing Circuits

Fig. 13 shows the structure of readout circuit in the simulation. The design of the readout circuit block diagram is shown in Fig. 25. In order to test the readout circuit, the sensed current is created based on experimental data from VNJ-P3HT diode sensors. Then the sensed current is used in three places. First, the Auto-Reset circuit reset the initial current information in voltage signals of peak-detector-and-hold circuit according to the variation of the sensed current (see 3.3.5). Second, the peak-detect-and-hold circuit gets the initial current information in voltage signals from the sensed current (see 3.3.2). Third, the divider uses the sensed current and the initial current information in voltage signals to output the ratio of saturation current to initial current (see 3.3.3). In the next, the saturation detector detect when the response is saturated by the output of divider (see 3.3.4). Finally, the logic gate decides whether or not to output the result according to the output of saturation detector and Auto-

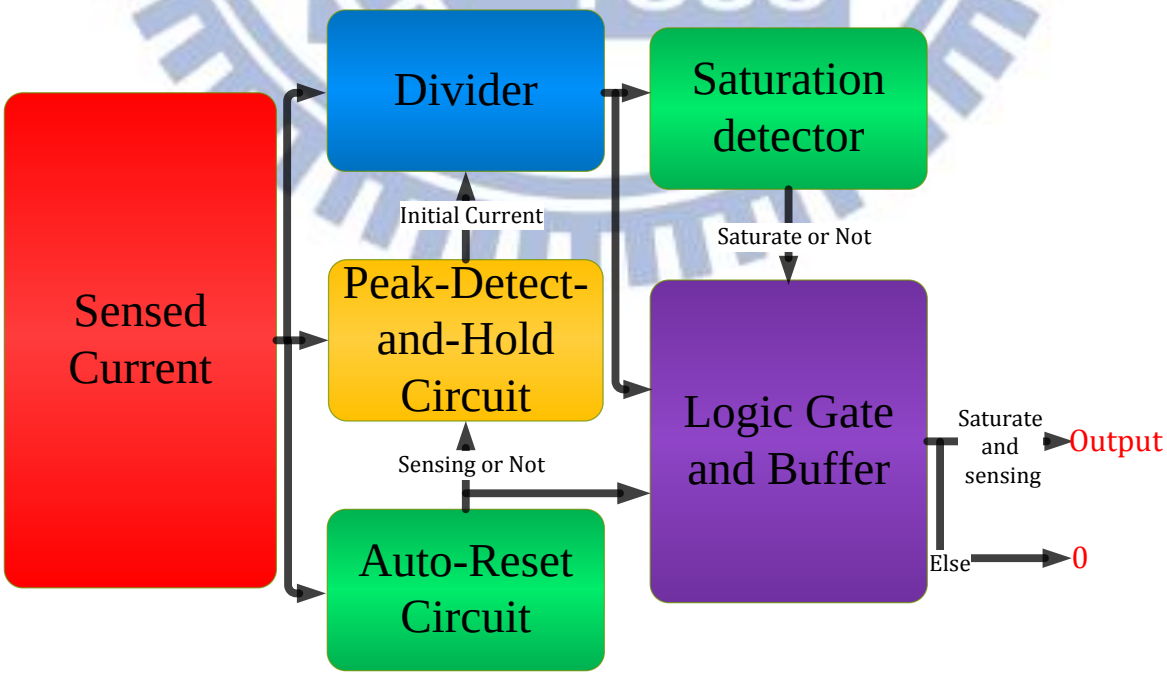

Fig. 25. Functional block diagram of readout circuit.

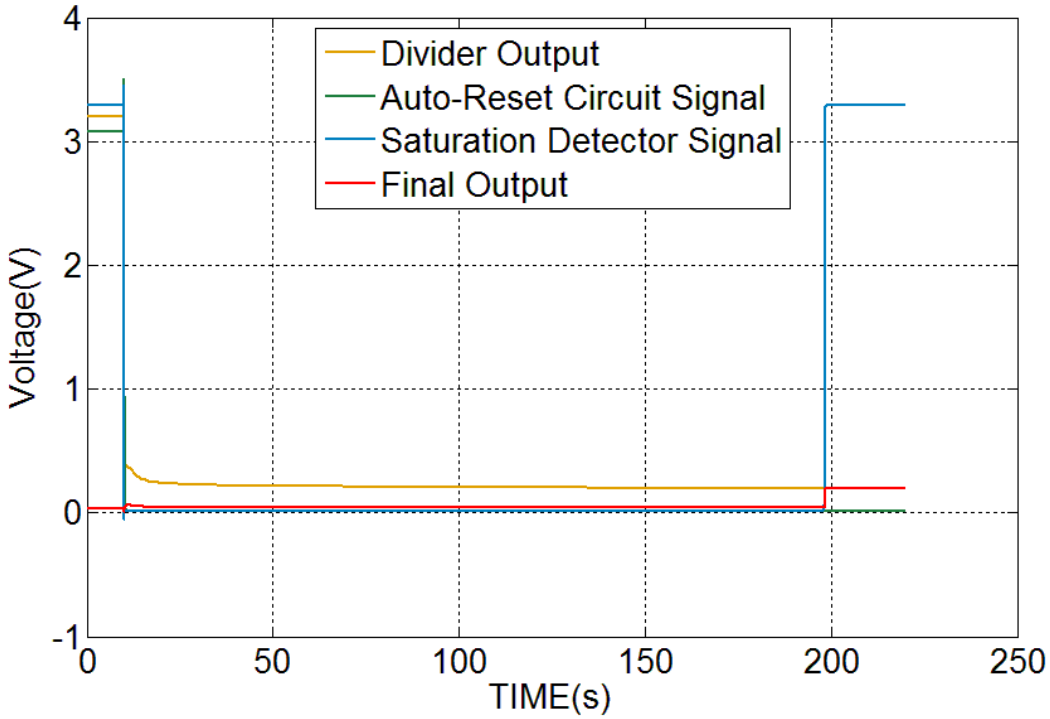

Fig. 26. The simulation results of readout circuit for single ammonia concentrations.

Reset circuit.

Fig. 26 shows the simulation results of readout circuit for single ammonia concentrations. Before sensing (0s~10s), the sensed current doesn't change. Thus the saturation detector considers the response is saturated and the output of saturation detector is high voltage level. Without a negative slope of the sensed current, the output of the auto-reset circuit is also high voltage level. When the VNJ-P3HT diode starts to interact with ammonia (10s~200s), the output of divider starts to decrease and the output of saturation detector switches to low voltage level. Due to the negative slope of the sensed current, the auto-reset circuit considers the response between sensor and ammonia start and the output of the auto-reset circuit also switches to low voltage level to hold the initial current information in voltage signals. So far, the final output has been low voltage level. After about 200 seconds, the response is saturated and the rate of change of sensed current is close to zero. Thus the saturation detector considers the response is saturated and the output of saturation detector switches to high voltage level. In chapter 3.3.6, the final output show the result only when the output of auto-reset circuit is

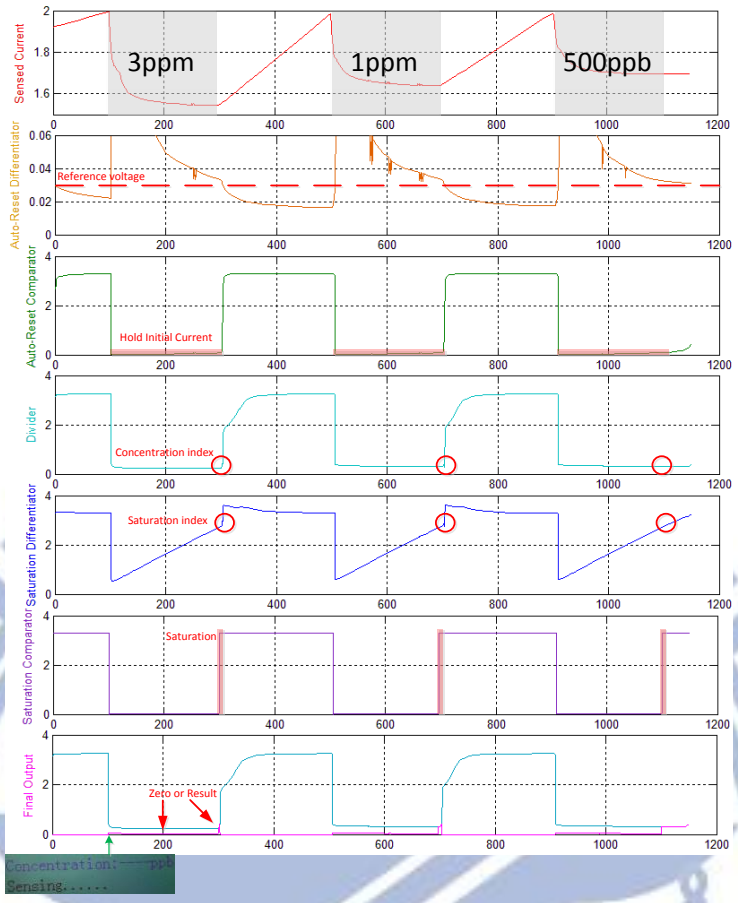

Fig. 27. The simulation results of readout circuit for several ammonia concentrations.

low voltage level and the output of saturation detector is high voltage level. The final output catches up with the output of divider to show the valuable data at this time.

Fig. 27 shows the simulation results of readout circuit for several ammonia concentrations (3ppm、1ppm、500ppb). When the response is saturated, ammonia is removed and the sensed current is on the increase. Thus the result is showed from final output for only a short time. The main principle of operation is the same as described previously. It is worth to mention that the auto-reset circuit automatically reset the initial current information in voltage signals of peak-detector-and-hold circuit (switches to high voltage level) when ammonia is removed and the sensed current is on the increase. The output of auto-reset circuit keeps the high voltage level until the next response start. This can prove the circuit can achieve automatic sensing.

4.2 Experimental Validation for Sensing Circuits

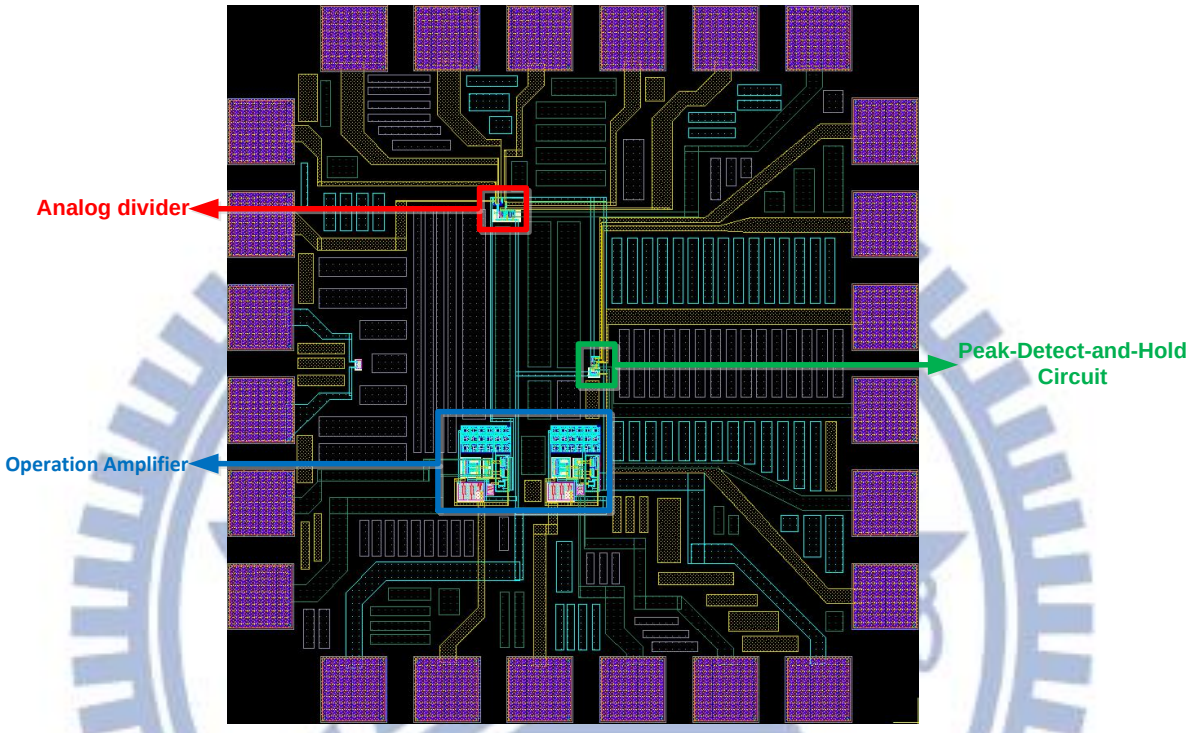

(a)

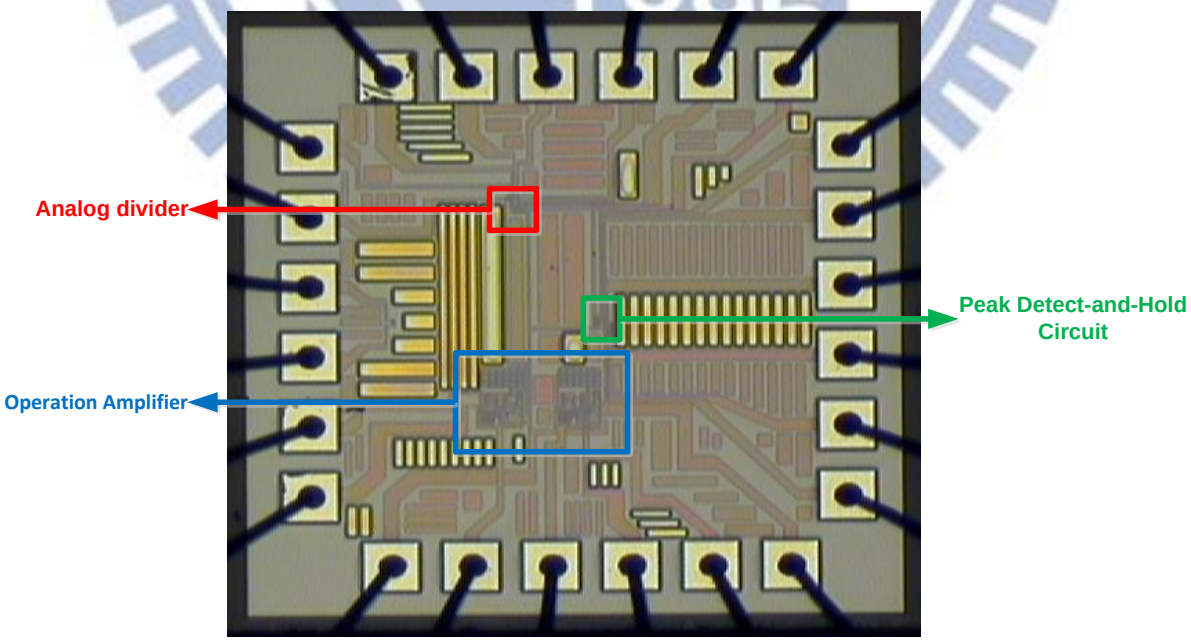

(b)

Fig. 28. (a) The layout (b) The photo of first IC.

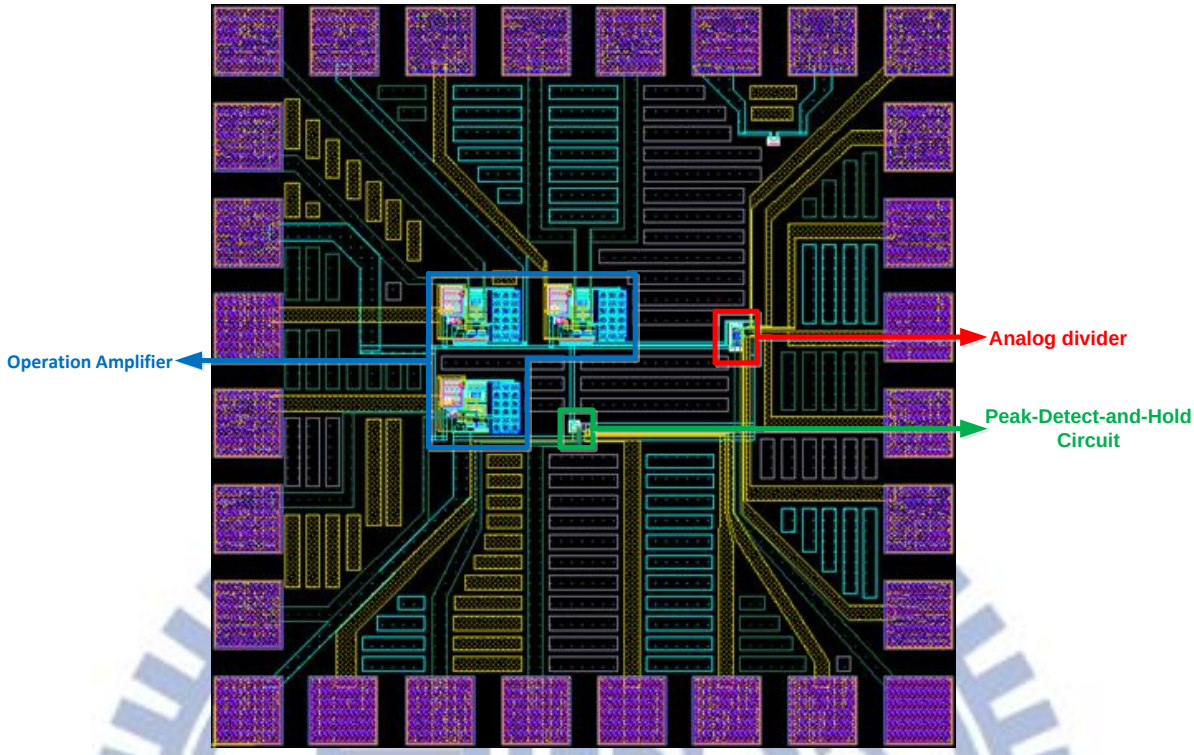

(a)

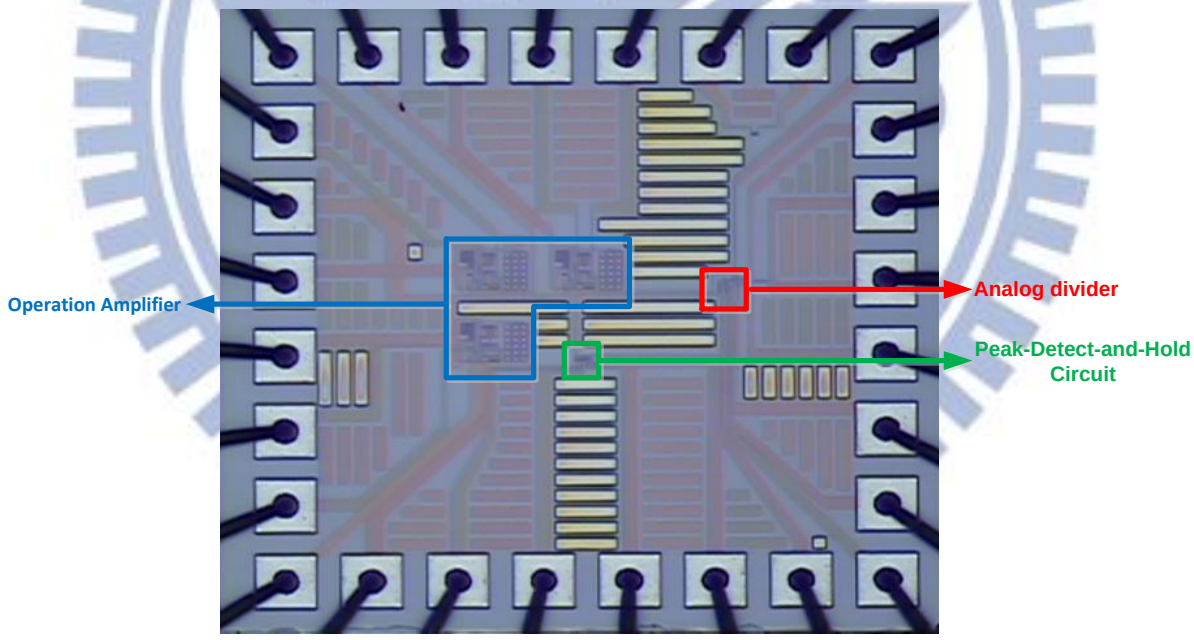

(b)

Fig. 29. (a) The layout (b) The photo of second IC.

Fig. 28 and Fig. 29 show the layout plot and the photo of the chip. Fig. 30 displays the layout plan of the third chip. The areas of ICs for the first, second and third chip are 1.083×1.04 mm^2, 1.082×1.082 mm^2 and 0.74×0.75 mm^2. The first IC has 24 pins, the second IC has 28 pins and

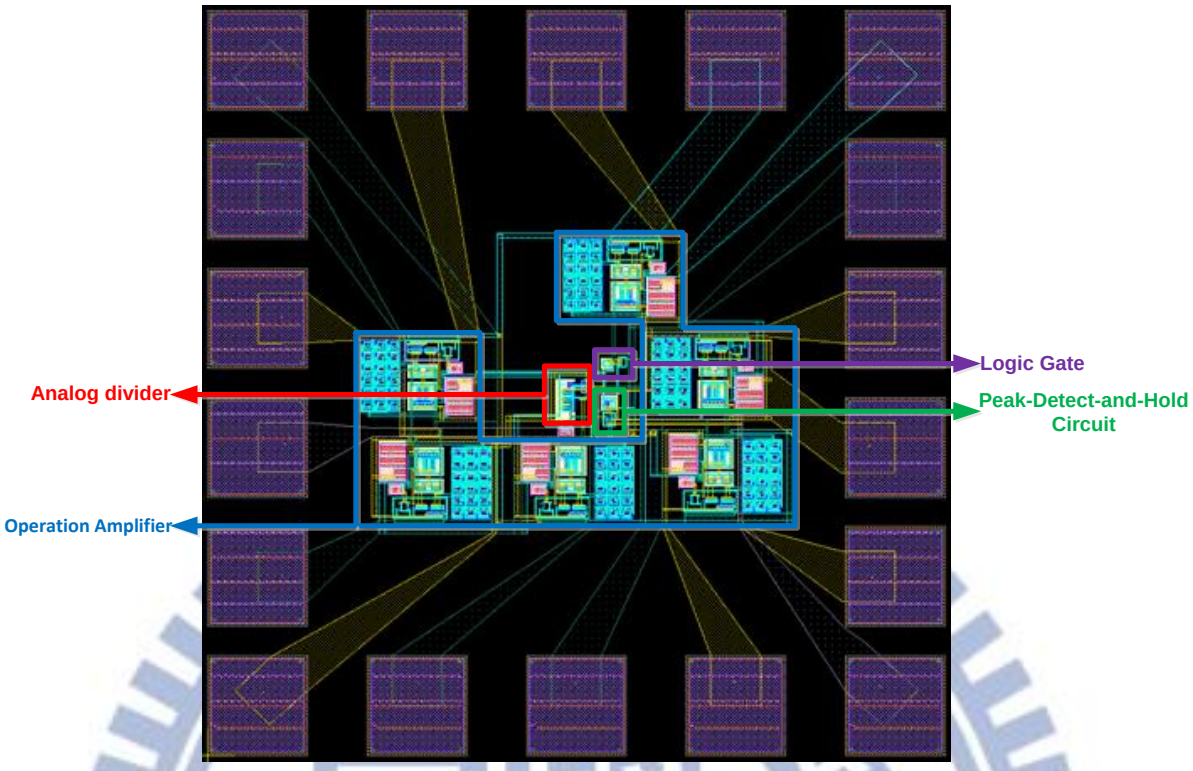

Fig. 30. The layout of third IC.

the third IC has 18 pins. This study implements the proposed circuits by TSMC 0.35um Mixed Signal 2P4M process. 3.3V is the supplied voltage of the circuit. Keithley Series 2400 Digital Source Meter generates the control signals and the entire circuit is measured.

4.2.1 The Sensing System

Because the readout circuit has to detect the difference between various signals about ammonia concentration, it is tested for sensing function first. The sensed current is created based on experimental data from VNJ-P3HT diode sensor to test the readout circuit. After constructing our own sweep by specifying the number of measure points and the source level at each point, Keithley Series 2400 Source Measure Unit (SMU) Instrument generates simulated sensing current. The analog output current of source meter are similar to sensed current in forms. The source meter is designed specifically for test applications that demand tightly coupled sourcing and measurement. It provides precision voltage and current sourcing as well as measurement capabilities. It is both a highly stable DC power source and a true

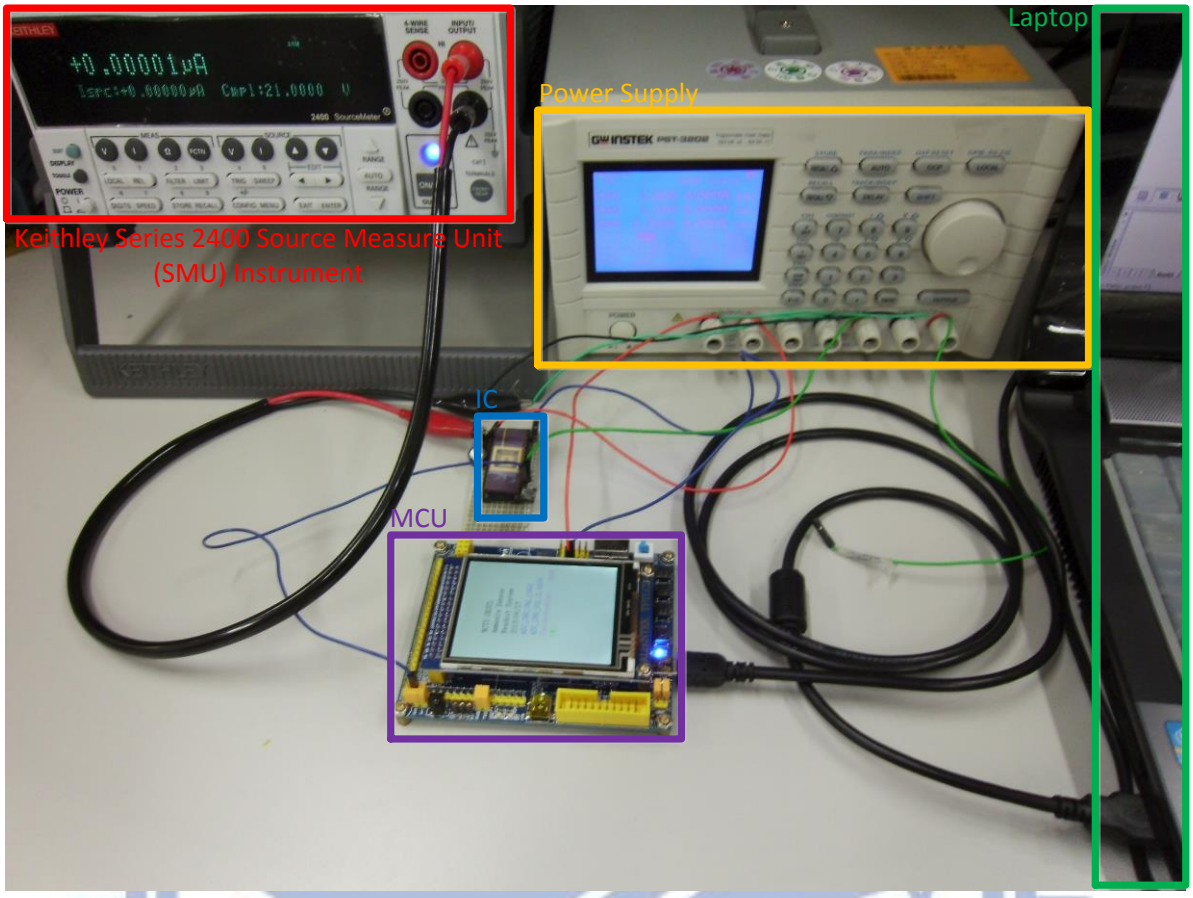

Fig. 31. The test environment of the sensing system.

instrument-grade 6½ -digit multi-meter. The power source characteristics include low noise, precision, and read-back. The multi-meter capabilities include high repeatability and low noise. The result is a compact, single-channel, DC parametric tester. In operation, it can be used as a voltage source, a current source, a voltage meter, a current meter, and an ohmmeter. Manufacturers of components and modules for the communications, semiconductor, computer, automotive, and medical industries will find the Source Meter SMU instruments invaluable for a wide range of characterization and production test applications.

The MCU is used to process the output of the readout circuit and estimate concentrations of ammonia. In order to search the corresponding concentration for output of the circuit, the programs create the data base. The analog-to-digital converter (ADC) is needed to transform analog output of circuit into digital input of MCU.

After presenting part of this system, the overall view of the sensing would be introduced.

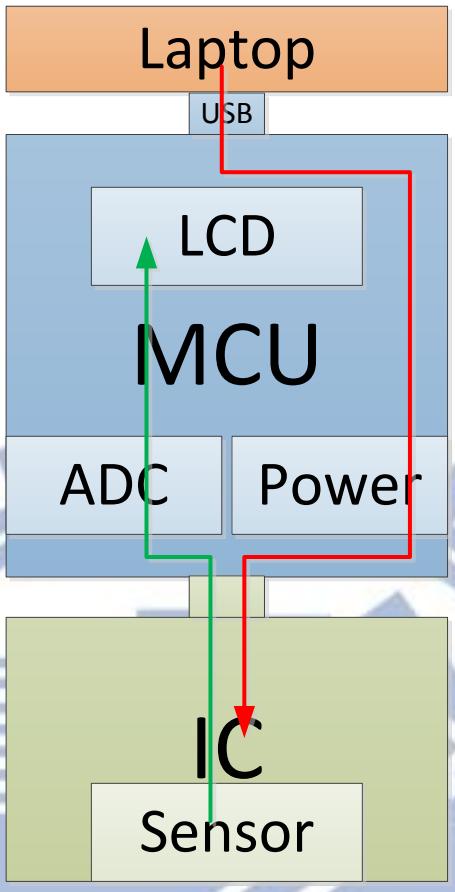

Fig. 32. The system configuration in a diagram.

The system configuration of test environment is exhibited in Fig. 31. The sensing system is composed of source meter, the sensing circuit, MCU and ADC devices. The following describes the process of the sensing system.

1. Keithley Series 2400 Source Measure Unit (SMU) Instrument acquires the experiment data based on ammonia sensor.

2. The proposal readout circuit processes the input signals related to the ammonia concentrations.

3. The ADC obtains the output signals of the readout circuit and transforms output signals of the sensing circuit into digital input of STM32.

4. In order to compute the corresponding concentrations, the STM32 processes the

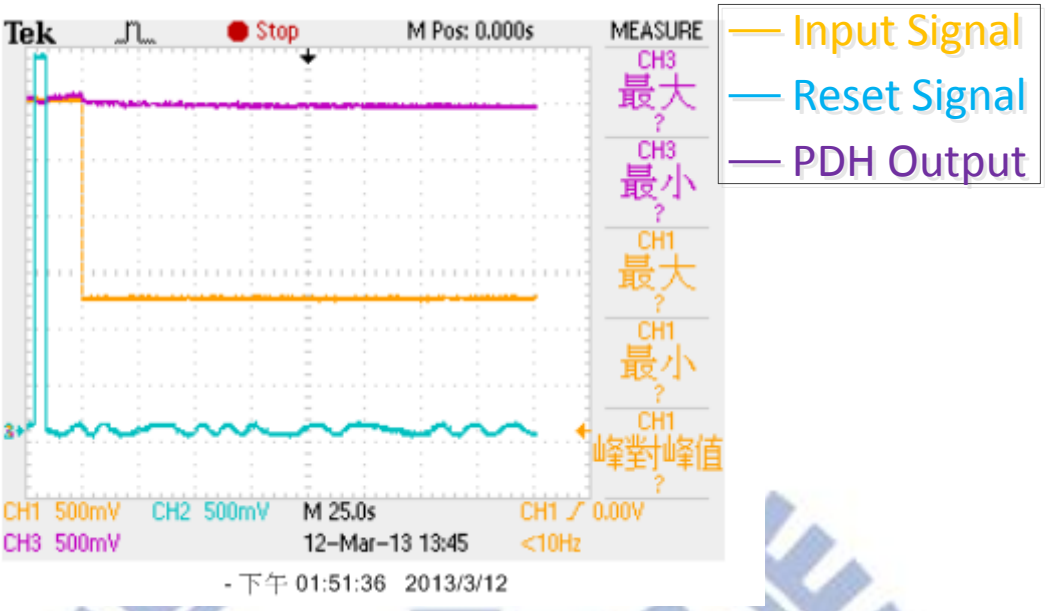

Fig. 33. The experimental results of the peak-detect-and-hold circuit.

digital input by programming.

Fig. 32 constructs the configuration of sensing system. The MCU board get its power (5V) from USB ports contained in laptops, cars, aircraft or even wall sockets. Then the MCU board provides power (3.3V) to the readout circuit. The LCD of MCU board real-time reveal the concentration of ammonia, which transformed from output of readout circuit by MCU.

4.2.2 Experimental Results of the Peak-Detect-and-Hold Circuit

It requires to verify that the peak-detect-and-hold circuit (shown in Fig. 16) can detect the initial current information in voltage signals and hold it for 200 seconds without the leakage current of capacitor first. This is an important difference to previous design which use MCU to hold the initial value. A current source dropped from 100μA~10μA created by Keithley Series 2400 Source Measure Unit (SMU) Instrument.

Fig. 33 shows the experimental results of the peak-detect-and-hold circuit. After resetting the output (the reset signal is “1”), the input is higher than the output. Thus the peak-detect-and-hold circuit start to detect the peak of input and hold it. Because our sensing time is 200

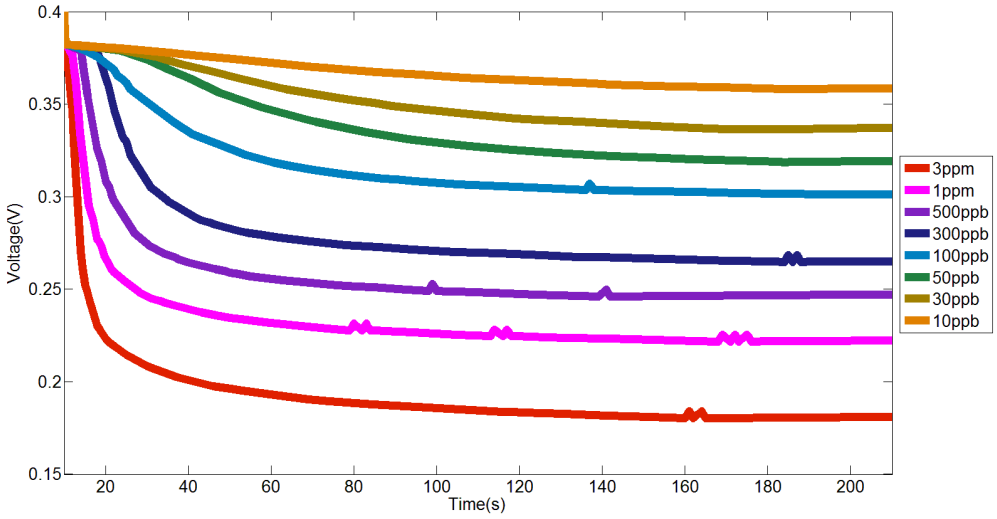

(a)

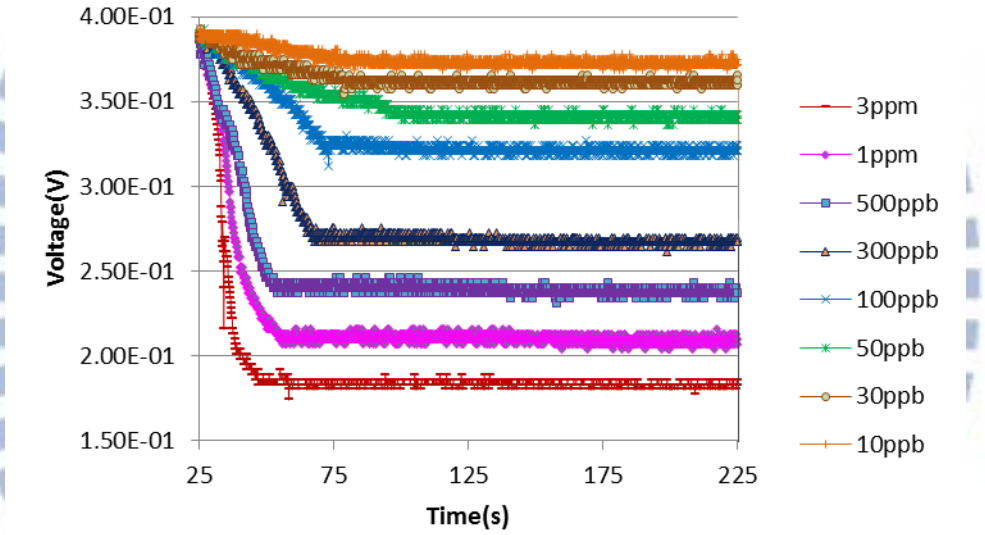

(b)

Fig. 34. (a) Post-simulation and (b) experimental results of analog divider with 10ppb ~ 3ppm of ammonia.

seconds, the super capacitor is used to hold the peak of the input without the leakage current. From Fig. 33, the peak-detect-and-hold circuit is workable and the super capacitor hold the peak for 200 seconds successfully. It can be used to get an initial value of the sensed current.

4.2.3 Applying Experimental Data of Ammonia Sensor and Experimental Results

With the peak-detect-and-hold circuit in function, the input voltage of divider is correct. The experimental setting is shown in Fig. 13. The VNJ-P3HT diode sensor is changed to the

Table II. The experimental results compared to post-simulation results.

Concentration(ppm)	Simulation result (V)	Experimental result (V)	Error (%)
0.01	0.359	0.375	4.266667
0.03	0.337	0.363	7.162534
0.05	0.319	0.339	5.899705
0.1	0.301	0.321	6.23053
0.3	0.265	0.267	0.749064
0.5	0.247	0.237	4.219409
1	0.222	0.207	7.246377
3	0.181	0.183	1.092896

Keithley Series 2400 Source Measure Unit (SMU) Instrument instead, which creates I_S. In previous chapters, Fig. 7 shows the original data of response in two hundred seconds. Eight ammonia concentrations for test are 10ppb, 30ppb, 50ppb, 0.1ppm, 0.3ppm, 0.5ppm, 1ppm and 3ppm. If the response multiplied by the initial current (I_O), values of the output current I_S will be decided. Fig. 34 shows the post-simulation and experimental output voltages of analog divider (V_O) in 0.01 ~ 3ppm ammonia. Table II shows the differences between experimental results with post-simulation results in 10ppb ~ 3ppm of ammonia. The differences are within 7.24%.

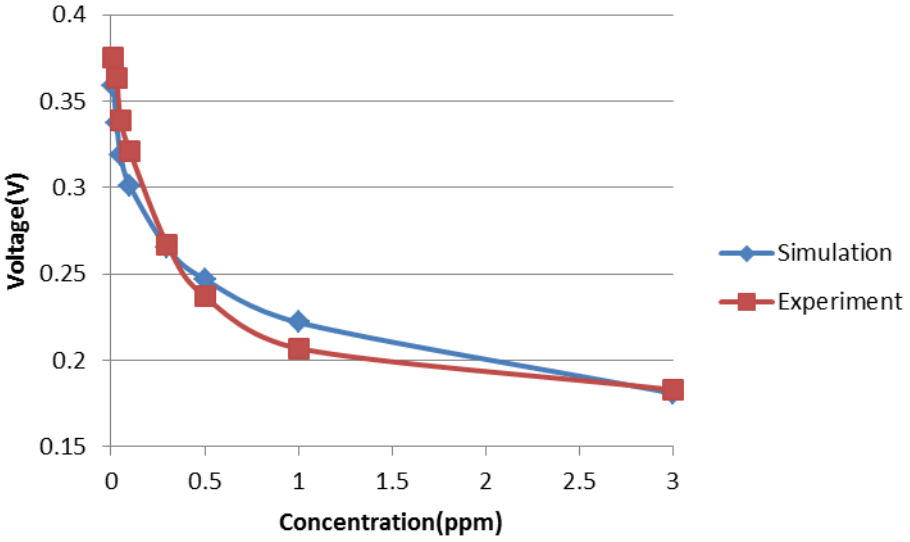

(a)

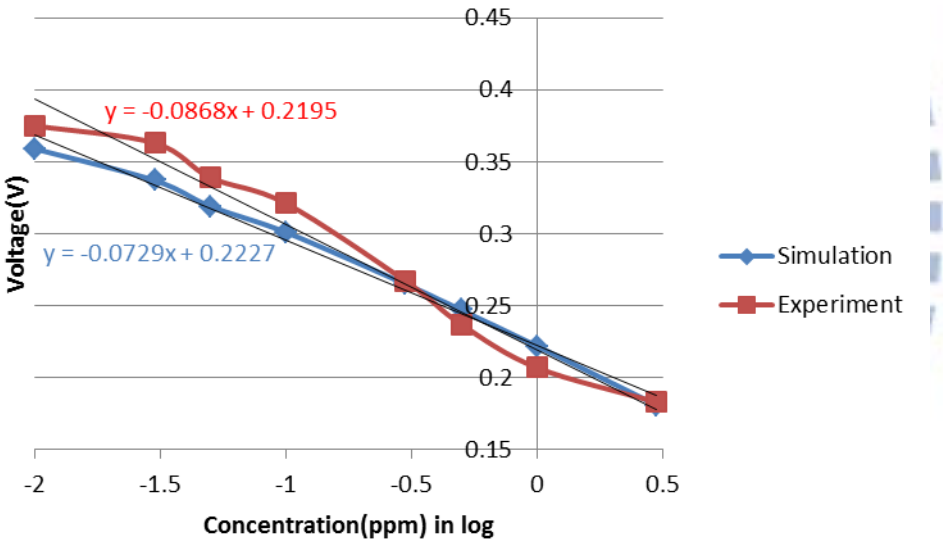

(b)

Fig. 35. Post-simulation and experimental output voltage in (a) 10ppb ~ 3ppm of ammonia, (b) 10ppb ~ 3ppm of ammonia in log scale.

Fig. 35(a) summarizes the relationship between the output voltage and concentration. With sets of experimental data collected on readout voltage and corresponding concentration levels in ppm, a linear relation is validated between logarithms of gas concentration level and output voltages of the readout circuit, as shown in Fig. 35(b). The resolution of the sensor achieves 86.8mV/log (ppm). The linear region is between -2~0.5ppm in log scale. The curves

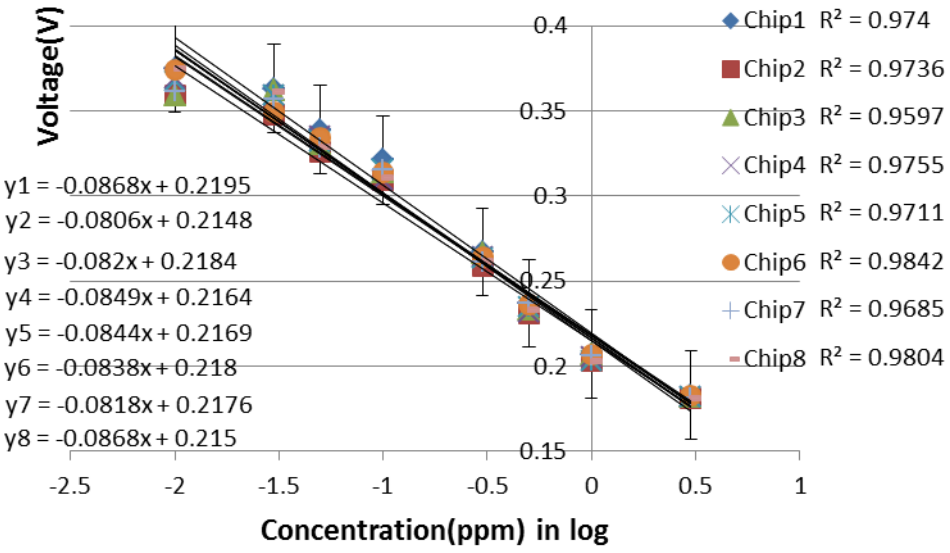

Fig. 36. The experimental output voltage of eight chips in 10ppb ~ 3ppm of ammonia in log scale.

can be approximated to linear equations, which based on simulation result is

$$y\ (x) = -0.0729 \log x + 0.2227 \tag{29}$$

and experimental result is

$$y\ (x) = -0.0868 \log x + 0.2195\,, \tag{30}$$

where y is output voltage of the analog divider, x is concentration of ammonia.

4.2.4 Reliability of Integrated Circuits

In previous charpters, this study verifies that the readout circuit can calculate the ratio of saturation current to initial current, which presents the specific gas concentration. Under manufacturing process variation, not all chips perform and maintain its functions. Before mass-production, the reliability of integrated circuits is very important. Fig. 36 shows the experimental output voltage of eight chips in 10ppb ~ 3ppm of ammonia in log scale, lines of eight results and the square of the residuals of the data after the fit. There are eight trend lines because of eight chips. The variation exist between chips.

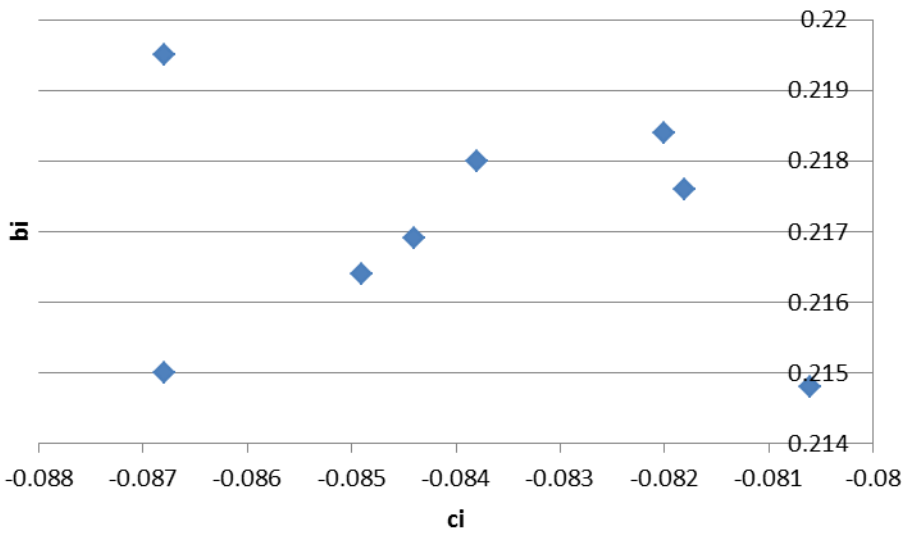

Fig. 37. The distribution of the parameters of the lines ($y_i = c_i x + b_i$).

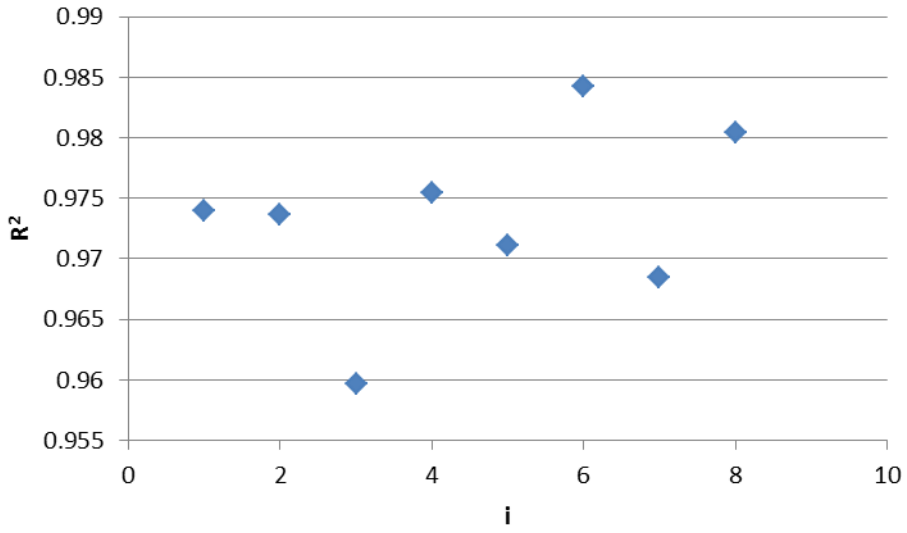

Fig. 38. The distribution of r-squared (R^2).

To analyze the variation, Fig. 37 shows the distribution of the parameters of the lines ($y_i = c_i x + b_i$). The range of b_i and c_i are 0.0047 and 0.0062, which can be ignored. Because not all points of data are on the lines, this study also tries to analyze the reliability of the lines. Fig. 38 shows the distribution of r-squared (R^2) which is the square of the residuals of the data after the fit. The R^2 value is basically a measure of how good the correlation is. The closer the R^2 value is to 1, the better the correlation. A good correlation between concentration in log and the output of divider indicates that the methodology is sound, and

that the readout circuit is working well. In other words, the higher the R^2, the better.

y_i are defined as the observed values and f_i are called the predicted values. In the below $\bar{y}$ is the mean of the observed data,

$$\bar{y} = \frac{1}{n}\sum_{i=1}^{n} y_i , \tag{31}$$

where n is the number of observations. The "variability" of the data set is measured through different sums of squares,

$$SS_{\text{tot}} = \sum_i (y_i - \bar{y})^2. \tag{32}$$

The total sum of squares (proportional to the sample variance) is

$$SS_{\text{reg}} = \sum_i (f_i - \bar{y})^2. \tag{33}$$

The regression sum of squares, also called the explained sum of squares is

$$SS_{\text{res}} = \sum_i (y_i - f_i)^2. \tag{34}$$

The sum of squares of residuals is also called the residual sum of squares. The most general definition of the coefficient of determination is

$$R^2 \equiv 1 - \frac{SS_{\text{res}}}{SS_{\text{tot}}} = \frac{SS_{\text{reg}}}{SS_{\text{tot}}}. \tag{35}$$

Generally speaking, an R^2 of 0.75 means that a reasonable correlation between the output of divider and concentration in log. 0.9 or above is very good. Fig. 36 shows a pretty good correlation. Because the line fits very nicely (R-squared over 0.9), this study can use it to estimate concentrations of ammonia.

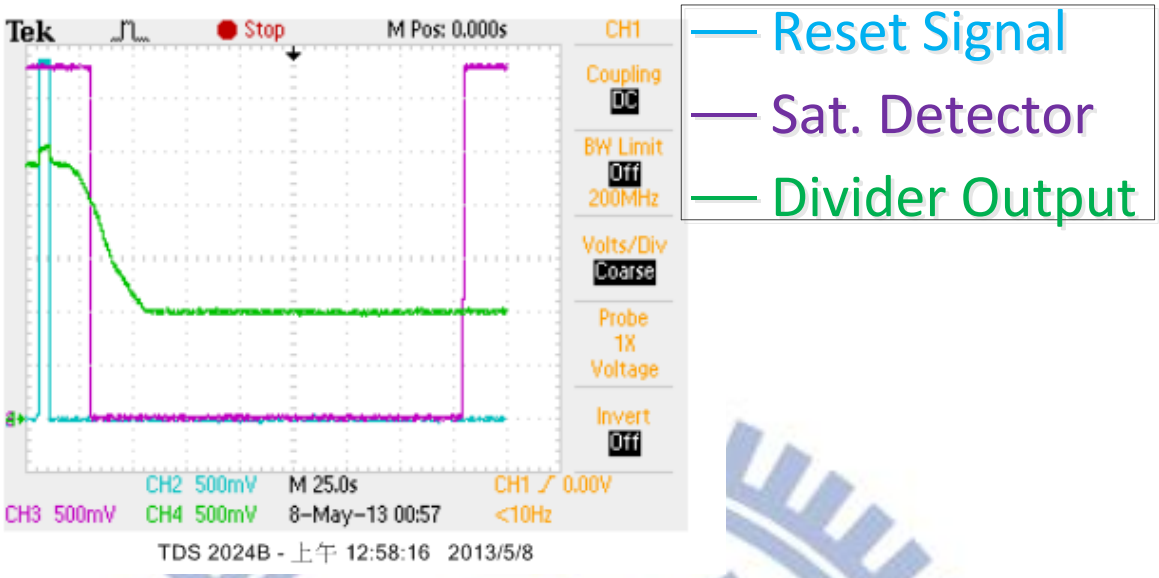

Fig. 39. The experimental results of the saturation detector.

4.2.5Experimental Results of the Saturation Detector

Having verified that the readout circuit can detect ammonia concentration accurately, this study tries to prove that the automatic readout circuit is workable. Fig. 26 shows the simulation results of readout circuit which can validate the automation of readout circuit. The experimental results of the saturation detector is shown in Fig. 39. The experimental setting is shown in Fig. 13 without auto-reset circuit, logic gate and buffer because the final version of the chip still in fabrication by National Chip Implementation Center. The VNJ-P3HT diode sensor is also changed to the Keithley Series 2400 Source Measure Unit (SMU) Instrument instead, which creates I_S.

In the beginning, the reset signal is “1” and the super capacitor of peak-detect-and-hold circuit discharged to ground voltage. Thus the denominator of divider get smaller and the output of divider get larger. When the reset signal switch to “0”, the capacitor starts to charge and hold the new peak. Until after this, the output of divider makes sense. Then the output of divider starts to decrease and the saturation detector judge that it is not saturated. Therefore the output of saturation detector switch to “0”. After about 200 seconds, the rate of change of

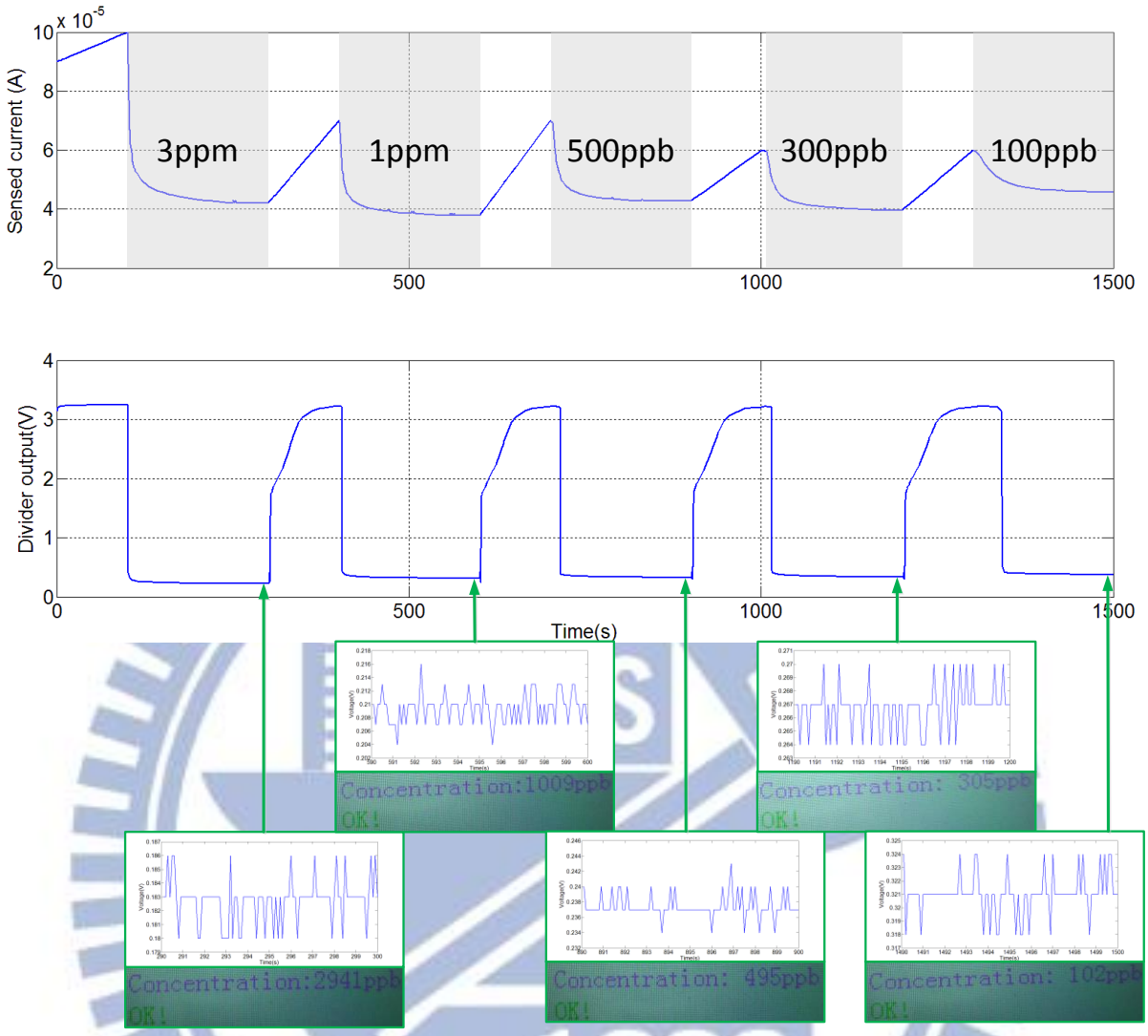

Fig. 40. The experimental results of LCD in 0.1 ~ 3ppm ammonia.

divider output is close to zero and the output of saturation detector switch to "1". The experiment of second chip verify that the readout circuit can automatically detect when the response is saturated.

4.2.6 Experimental Results of MCU

With the readout circuit in function, the output of analog circuit connect to the ADC of MCU. Then the data is processed using a MCU to estimate concentrations of ammonia. Finally, the concentration of ammonia is displayed on the LCD. Fig. 40 contrasts the experimental results of LCD with waveform. At the bottom of Fig. 27, the output show the result only when sensor

Table III. The specifications of readout circuit.

Specifications	Values
Power Supply (VDD)	3.3V
Power consumption	4.6mW
Input Range of Sensing Current	0μA~100μA
Input Range of Sensing Voltage	1.5V~3.3V
Range of Bias Voltage	1.5V~3V
Resolution	86.8mV/ log(ppm)
Process of Manufacturing	0.35μm 2P4M 3.3V mixed-signal CMOS process
Die Area	0.74×0.75 mm^2

react with gas and the current saturate, otherwise the output display zero because of the logic gate. The valid output is varied in the range between 0.15V and 0.4V (see Fig. 34). As show in the Fig. 27, if the output of readout circuit is lower than 0.15 voltage, "----ppb" and "Sensing……" are displayed on the LCD. This situation represents an unsaturated result.

On the other hand, the LCD accurately shows the results in 0.1ppm, 0.3ppm, 0.5ppm, 1ppm and 3ppm ammonia, as shown in Fig. 40. Even though the initial current changes, the readout circuit obtains the new initial value and outputs the correct results. This indicates the readout system is workable. Table III shows the overall specifications of readout circuit.

CHAPTER 5

Conclusions and Future works

An automatic readout circuit for gas sensor is proposed in this study. These analog IC are realized by the TSMC 0.35um Mixed-Signal 2P4M process. The circuit is designed, implemented and validated by the experimental output currents of the readout circuit which varies with sensed currents.

The circuit is connected externally to the sensors that output the current varying with the concentration of target gas, although the ammonia sensors based on VNJ-P3HT diode are not integrated into a single chip with the readout circuit. In order to perform experiments in a more convenient and efficient way, Keithley Series 2400 Source Measure Unit (SMU) Instrument is chosen to simulate the output current of the front-end VNJ-P3HT diode device in experiments. Finally, the sensing system is able to detect minimum ammonia concentration of 10ppb, while the maximum one reaches around 3ppm.

Without the AD/DA of MCU in the previous design, the peak-detect-and-hold circuit is used to holds the input value of the analog divider. The ratio of saturation current to initial current can be calculated by the analog divider and present the specific gas concentration. Thus the problem that the initial current varies from time to time is solved. The auto-reset circuit for detecting transitions between different gas concentration levels is designed and implemented in this study for sensing automation. The design of the proposed saturation detector and logic gate can provide more convenience for real-time detection of gas concentration.

With sets of experimental data collected on readout voltage and corresponding concentration levels in ppm, a linear relation is validated between logarithms of gas concentration level and output voltages of the readout circuit. The linear equations of the

Fig. 41. The imaginary figure.

analog divider's output voltage versus concentration of ammonia in log scale are determined. The resolution of the sensor achieves 86.8mV/log (ppm). This relation is utilized further in a micro-processor for calculating gas concentration level in ppb. Finally, the gas concentration level in ppm is displayed on a LCD panel. The experimental results show that errors are within 7.24%.

The size of MCU can be further reduced in future works. Then the entire system (analog IC, MCU and LCD) can be fabricated to a compact module. The imaginary figure is shown in Fig. 41. Finally, the resolution and the linear range of the readout circuit's output about the ammonia concentration can be further improved.

APPENDIX

Table IV. The design parameters of readout circuit.

Transistors	Aspect ratio (μm/μm)	m	Transistors	Aspect ratio (μm/μm)	m
M1-M6	10/4	1	M3p,M4p	10/1	2
M7-M10	25/5	2	M5p	10/1	9
M10	20/2	1	M6p	1/1	10
M1p,M2p	2/1	1	M7p, M8p	3/1	1

Resistance	Ω	Capacitance	F
R_0	8k	C_0	1p

REFERENCES

[1] M. Kikuchi, K. Omori, and S. Shiratori, "Quartz crystal microbalance (QCM) sensor for ammonia gas using clay/polyelectrolyte layer-by-layer self-assembly film," *Proceedings of IEEE Sensors*, pp. 718-721 vol.2, 24-27 Oct. 2004.

[2] C.-Y. Shen, C.-L. Hsu, and D.-L. Wang, "Shear Horizontal Surface Acoustic Wave Sensors Based on Polyaniline for Ammonia Gas Sensing," *EuroSime 2006. 7th International Conference on Thermal, Mechanical and Multiphysics Simulation and Experiments in Micro-Electronics and Micro-Systems*, pp. 1-3, 24-26 April 2006.

[3] C.-Y. Shen, C.-P. Huang, and W.-T. Huang, "The detection properties of ammonia SAW gas sensors based on L-glutamic acid hydrochloride," *IEEE Transactions on Ultrasonics, Ferroelectrics and Frequency Control*, vol. 52, pp. 1877-1880, 2005.

[4] S. O'Keeffe, H. Manap, G. Dooly, and E. Lewis, "Real-time monitoring of agricultural ammonia emissions based on optical fibre sensing technology," *IEEE Sensors*, pp. 1140-1143, 1-4 Nov. 2010.

[5] T. Shiquan, J. C. Fanguy, and T. V. S. Sarma, "A Fiber-Optic Sensor for Monitoring Trace Ammonia in High-Temperature Gas Samples With a CuCl2 -Doped Porous Silica Optical Fiber as a Transducer," *IEEE Sensors Journal*, vol. 8, pp. 2000-2007, 2008.

[6] M. Shan, X. Li, C. Zhu, and J. Zhang, "Gas concentration detection using ultrasonic based on wireless sensor networks," *2nd International Conference on Information Science and Engineering (ICISE)*, pp. 2101-2106, 4-6 Dec. 2010.

[7] T.-Y. Chen, H.-I. Chen, Y.-J. Liu, C.-C. Huang, C.-S. Hsu, C.-F. Chang, *et al.*, "Ammonia Sensing Properties of a Pt/AlGaN/GaN Schottky Diode," *IEEE Transactions on Electron Devices*, vol. 58, pp. 1541-1547, 2011.

[8] H. Wingbrant, M. Persson, A. E. Abom, M. Eriksson, B. Andersson, S. Simko, *et al.*, "Cosputtered Metal and SiO2 Layers for Use in Thick-Film MISiC NH3 Sensors," *IEEE Sensors Journal*, vol. 6, pp. 887-897, 2006.

[9] A. D. Aguilar, E. S. Forzani, L. A. Nagahara, I. Amlani, R. Tsui, and N. J. Tao, "A Breath Ammonia Sensor Based on Conducting Polymer Nanojunctions," *IEEE Sensors Journal*, vol. 8, pp. 269-273, 2008.

[10] H.-W. Zan, M.-Z. Dai, T.-Y. Hsu, H.-C. Lin, H.-F. Meng, and Y.-S. Yang, "Porous Organic TFTs for the Applications on Real-Time and Sensitive Gas Sensors," *IEEE Electron Device Letters*, vol. 32, pp. 1143-1145, 2011.

[11] S.-L. Liu, Y.-C. Zhang, X.-Y. Meng, W.-G. Lu, and Z.-J. Chen, "A design of readout circuit for 384×288 uncooled microbolometer infrared focal plane array," *IEEE 11th International Conference on Solid-State and Integrated Circuit Technology (ICSICT)*, pp. 1-3, Oct. 29 -Nov. 1 2012.

[12] Y. Yang, "Effective readout pixel sensor circuit design for infrared focal plane array and three-dimension image MEMS VLSI system," *International SoC Design Conference (ISOCC)*, pp. 286 - 289, 17-18 Nov. 2011.

[13] H. Zhao, Y. Zhao, Y. Song, J. Liao, and J. Geng, "A low power cryogenic CMOS ROIC for 512×512 infrared focal plane array," *International Conference of Electron Devices and Solid-State Circuits (EDSSC)*, pp. 1-2, 17-18 Nov. 2011.

[14] T. Yin, H. Wu, Q. Wu, H. Yang, and J. Jiao, "A TIA-based readout circuit with temperature compensation for MEMS capacitive gyroscope," *IEEE International Conference on Nano/Micro Engineered and Molecular Systems (NEMS)*, pp. 401-405, 20-23 Feb. 2011.

[15] T. Yin, H. Wu, Q. Wu, H. Yang, and J. Jiao, "A TIA-based interface for MEMS capacitive gyroscope," *IEEE 9th International Conference on ASIC (ASICON)*, pp. 149-152, 25-28 Oct. 2011.

[16] T.-T. Chen, J.-C. Huang, Y.-C. Peng, C.-H. Chu, C.-H. Lin, C.-W. Cheng, *et al.*, "A 17.6-MHz 2.5V ultra-low polarization voltage MEMS oscillator using an innovative high gain-bandwidth fully differential trans-impedance voltage amplifier," *IEEE 26th International Conference on Micro Electro Mechanical Systems (MEMS)*, pp. 741-744, 20-24 Jan. 2013.

[17] Y.-W. Chang, P.-C. Yu, Y.-T. Huang, and Y.-S. Yang, "A High-Sensitivity CMOS-Compatible Biosensing System Based on Absorption Photometry," *IEEE Sensors Journal*, vol. 9, pp. 120-127, 2009.

[18] H.-W. Zan, W.-W. Tsai, Y.-r. Lo, Y.-M. Wu, and Y.-S. Yang, "Pentacene-Based Organic Thin Film Transistors for Ammonia Sensing," *IEEE Sensors Journal*, vol. 12, pp. 594-601, 2012.

[19] M.-Z. Dai, Y.-L. Lin, H.-C. Lin, H.-W. Zan, K.-T. Chang, H.-F. Meng, *et al.*, "Highly Sensitive Ammonia Sensor with Organic Vertical Nanojunctions for Noninvasive Detection of Hepatic Injury," *Analytical Chemistry*, vol. 85, pp. 3110-3117, 03/19 2013.

[20] W.-J. Lin, P. C. P. Chao, S.-K. Lin, and H.-W. Zan, "A novel readout circuit for an OTFD gas sensor with a new front-end trans-impedance amplifier," *IEEE Sensors Journal*, pp. 1141-1144, 28-31 Oct. 2011.

[21] W.-C. Lin, "A Front-end Readout Circuit Including an Analog Divider for an OTFT Gas Sensor," *Institute of Electrical and Control Engineering*, vol. Master, July 2012.

[22] M. A. Al-Absi, "Low-voltage and low-power CMOS current-mode divider and 1/x circuit," *Intl Conf on Electronic Devices, Systems and Applications (ICEDSA)*, pp. 245-247, 11-14 April 2010.

[23] L. W and L. S-I, "CMOS Tunable 1/x Circuit and Its Applications," *IEICE Trans Fundam Electron Commun Comput Sci (Inst Electron Inf Commun Eng)*, vol. E86-A, pp. 1896-1899, 2003.

[24] X. L. Zhang and P. K. Chan, "An untrimmed CMOS amplifier with high CMRR and low offset for sensor applications," *APCCAS 2008. IEEE Asia Pacific Conference on Circuits and Systems*, pp. 802-805, Nov. 30 - Dec. 3 2008.

[25] "STM32 User Manual Rev. 2.3," April 2013.